[redacted]

39

NASA TECHNICAL MEMORANDUM

NASA TM X-894

NASA TM X-894

LOW-SPEED STATIC AND OSCILLATORY STABILITY CHARACTERISTICS OF A MODEL OF THE APOLLO LAUNCH-ESCAPE VEHICLE AND COMMAND MODULE

by Peter C. Boisseau
Langley Research Center
Langley Station, Hampton, Va.

[redacted]

NATIONAL AERONAUTICS AND SPACE ADMINISTRATION • WASHINGTON, D. C. • OCTOBER 1963

[redacted]

TECHNICAL MEMORANDUM X-894

LOW-SPEED STATIC AND OSCILLATORY STABILITY CHARACTERISTICS OF A MODEL OF THE APOLLO LAUNCH-ESCAPE VEHICLE AND COMMAND MODULE

By Peter C. Boisseau

Langley Research Center
Langley Station, Hampton, Va.

NATIONAL AERONAUTICS AND SPACE ADMINISTRATION

NATIONAL AERONAUTICS AND SPACE ADMINISTRATION

TECHNICAL MEMORANDUM X-894

LOW-SPEED STATIC AND OSCILLATORY STABILITY CHARACTERISTICS OF A MODEL OF THE APOLLO LAUNCH-ESCAPE VEHICLE AND COMMAND MODULE*

By Peter C. Boisseau

SUMMARY

A force-test investigation has been conducted at the Langley Research Center to provide some information on the longitudinal and lateral stability characteristics at low subsonic speeds of a 1/7-scale model of the Apollo launch-escape vehicle and command module. The model in all configurations had at least neutral static longitudinal and directional stability near zero angle of attack. The launch-escape vehicle had stable values of damping in pitch but unstable values of damping in yaw near zero angle of attack, whereas the command module in the exit attitude had very small values of damping in pitch and yaw.

INTRODUCTION

An investigation is being conducted by the National Aeronautics and Space Administration to provide information on the stability characteristics of the Apollo spacecraft over the speed range from subsonic to supersonic (for example, see refs. 1 and 2). The present investigation was made to provide some information on the longitudinal and lateral stability characteristics at low subsonic speeds of a 1/7-scale model of the Apollo launch-escape vehicle and command module.

Static and dynamic force tests were made with the launch-escape vehicle over an angle-of-attack range from -30° to 60°. Similar tests were made of the command module in the exit attitude over an angle-of-attack range from 0° to 180°. Only static force tests were made of the command module in the reentry attitude over an angle-of-attack range from 0° to 180°. The models were also tested over an angle-of-sideslip range from -20° to 20°. The data are presented with a minimum of analysis.

*Title, Unclassified.

SYMBOLS

The positive direction of forces and moments is shown in figure 1. The data are referred to the body system of axes originating at the center of gravity (see fig. 2). All measurements are reduced to standard coefficient form and are based on the maximum diameter and cross-sectional area of the command module.

A maximum cross-sectional area perpendicular to X body axis, sq ft

C_A axial-force coefficient, $\frac{\text{Axial force}}{q_\infty A}$

C_D drag coefficient, $\frac{\text{Drag}}{q_\infty A}$

C_L lift coefficient, $\frac{\text{Lift}}{q_\infty A}$

C_l rolling-moment coefficient, $\frac{\text{Rolling moment}}{q_\infty A d}$

C_{l_β} effective dihedral parameter, $\left(\frac{\Delta C_l}{\Delta \beta}\right)_{\beta=\pm 5^\circ}$

$\Delta C_l, \Delta C_n, \Delta C_Y$ incremental force and moment coefficients

C_m pitching-moment coefficient, $\frac{\text{Pitching moment}}{q_\infty A d}$

C_N normal-force coefficient, $\frac{\text{Normal force}}{q_\infty A}$

C_n yawing-moment coefficient, $\frac{\text{Yawing moment}}{q_\infty A d}$

C_{n_β} directional-stability parameter, $\left(\frac{\Delta C_n}{\Delta \beta}\right)_{\beta=\pm 5^\circ}$

C_Y lateral-force coefficient, $\frac{\text{Lateral force}}{q_\infty A}$

C_{Y_β} side-force parameter, $\left(\frac{\Delta C_Y}{\Delta \beta}\right)_{\beta=\pm 5^\circ}$

d maximum body diameter, ft

F_Y side force, lb

k reduced-frequency parameter, $\frac{\omega d}{2V}$

M_X rolling moment, ft-lb

M_Z yawing moment, ft-lb

q pitching angular velocity, radians/sec

$\dot{q}$ rate of change of pitching angular velocity, radians/sec^2

q_∞ free-stream dynamic pressure, lb/sq ft

R Reynolds number

r yawing velocity, radians/sec

V free-stream velocity, ft/sec

X, Y, Z body reference axes

α angle of attack of model center line, deg

$\dot{\alpha}$ rate of change of angle of attack, radians/sec

β angle of sideslip, deg

ω circular frequency of oscillation, radians/sec

$$C_{A_q} = \frac{\partial C_A}{\partial\left(\frac{qd}{2V}\right)} \qquad C_{m_q} = \frac{\partial C_m}{\partial\left(\frac{qd}{2V}\right)} \qquad C_{N_q} = \frac{\partial C_N}{\partial\left(\frac{qd}{2V}\right)}$$

$$C_{A_{\dot{q}}} = \frac{\partial C_A}{\partial\left(\frac{\dot{q}d^2}{4V^2}\right)} \qquad C_{m_{\dot{q}}} = \frac{\partial C_m}{\partial\left(\frac{\dot{q}d^2}{4V^2}\right)} \qquad C_{N_{\dot{q}}} = \frac{\partial C_N}{\partial\left(\frac{\dot{q}d^2}{4V^2}\right)}$$

$$C_{A_\alpha} = \frac{\partial C_A}{\partial \alpha} \qquad C_{m_\alpha} = \frac{\partial C_m}{\partial \alpha} \qquad C_{N_\alpha} = \frac{\partial C_N}{\partial \alpha}$$

$$C_{A_{\dot{\alpha}}} = \frac{\partial C_A}{\partial\left(\frac{\dot{\alpha}d}{2V}\right)} \qquad C_{m_{\dot{\alpha}}} = \frac{\partial C_m}{\partial\left(\frac{\dot{\alpha}d}{2V}\right)} \qquad C_{N_{\dot{\alpha}}} = \frac{\partial C_N}{\partial\left(\frac{\dot{\alpha}d}{2V}\right)}$$

$$C_{l_r} = \frac{\partial C_l}{\partial\left(\frac{rd}{2V}\right)} \qquad C_{n_r} = \frac{\partial C_n}{\partial\left(\frac{rd}{2V}\right)} \qquad C_{Y_r} = \frac{\partial C_Y}{\partial\left(\frac{rd}{2V}\right)}$$

$$C_{l_{\dot{r}}} = \frac{\partial C_l}{\partial\left(\frac{\dot{r}d^2}{4V^2}\right)} \qquad C_{n_{\dot{r}}} = \frac{\partial C_n}{\partial\left(\frac{\dot{r}d^2}{4V^2}\right)} \qquad C_{Y_{\dot{r}}} = \frac{\partial C_Y}{\partial\left(\frac{\dot{r}d^2}{4V^2}\right)}$$

$$C_{l_{\dot{\beta}}} = \frac{\partial C_l}{\partial\left(\frac{\dot{\beta}d}{2V}\right)} \qquad C_{n_{\dot{\beta}}} = \frac{\partial C_n}{\partial\left(\frac{\dot{\beta}d}{2V}\right)} \qquad C_{Y_{\dot{\beta}}} = \frac{\partial C_Y}{\partial\left(\frac{\dot{\beta}d}{2V}\right)}$$

A dot over a symbol denotes a derivative with respect to time.

DEFINITION OF DERIVATIVES

In the present investigation the term in-phase derivative refers to any one of the oscillatory derivatives that are based on the components of forces and moments in phase with the angle of pitch or yaw produced in the oscillatory tests. The term out-of-phase derivative refers to any one of the stability derivatives that is based on the components of forces and moments 90° out of phase with the angle of pitch or yaw. The oscillatory derivatives of the present investigation were measured in the following combinations:

$C_{m_\alpha} - k^2 C_{m_{\dot{q}}}$

$C_{A_\alpha} - k^2 C_{A_{\dot{q}}}$ } In-phase pitching derivatives, per radian

$C_{N_\alpha} - k^2 C_{N_{\dot{q}}}$

$C_{m_q} + C_{m_{\dot{\alpha}}}$

$C_{A_q} + C_{A_{\dot{\alpha}}}$ } Out-of-phase pitching derivatives, per radian

$C_{N_q} + C_{N_{\dot{\alpha}}}$

$C_{l_\beta} \cos \alpha + k^2 C_{l_{\dot{r}}}$

$C_{n_\beta} \cos \alpha + k^2 C_{n_{\dot{r}}}$ } In-phase yawing derivatives, per radian

$C_{Y_\beta} \cos \alpha + k^2 C_{Y_{\dot{r}}}$

$C_{l_r} - C_{l_{\dot{\beta}}} \cos \alpha$

$C_{n_r} - C_{n_{\dot{\beta}}} \cos \alpha$ } Out-of-phase yawing derivatives, per radian

$C_{Y_r} - C_{Y_{\dot{\beta}}} \cos \alpha$

MODEL AND APPARATUS

Drawings and photographs of the configurations tested are presented in figures 2 and 3, respectively. The model was constructed of aluminum and steel tubing and was fabricated in such a way that the escape tower could be removed from the command module (see fig. 3(b)), thus providing the various configurations used in the investigation. The escape tower could also be fitted with a 9.30-inch-diameter disk at the base of the rocket. (See figs. 2(a) and 3(c).)

The tests were conducted in a low-speed wind tunnel with a 12-foot octagonal test section at the Langley Research Center. The apparatus and technique used in the tests are described in reference 3.

TESTS

Static and dynamic force tests were made to determine the longitudinal and lateral stability characteristics of the launch-escape vehicle over an angle-of-attack range from -30° to 60°. Similar tests were also made for the command module in the exit attitude over an angle-of-attack range from 0° to 180°. Only static force tests were made of the command module in the reentry attitude.

The force tests were made at a dynamic pressure of 4.05 pounds per square foot which corresponds to an airspeed of about 59 feet per second at standard sea-level conditions and to a test Reynolds number of about 0.68×10^6 based on the maximum diameter of the command module. Most of the dynamic force tests were made in pitch and yaw for amplitudes of ±5° and for a reduced-frequency parameter k of about 0.6. For a few of the dynamic tests the amplitude was varied up to a maximum of ±30°.

PRESENTATION OF RESULTS

The static longitudinal and lateral data for the launch-escape vehicle and command module are presented in figures 4 to 12, and the oscillatory data for both configurations are presented in figures 13 to 17.

Static Derivatives

The data of figure 4 indicate that the launch-escape vehicle was trimmed in pitch at an angle of attack of about 5° and was statically stable longitudinally about this trim point over an angle-of-attack range from about -25° to 20°. The data also show that the disk had only a small effect on the pitching-moment and normal-force characteristics but had an appreciable effect on axial force. Since some of the data have a nonlinear variation with angle of sideslip, the lateral-stability parameters presented in figure 7 should be used only to give an indication of the trends in the lateral stability characteristics of the launch-escape vehicle. The values of these parameters were obtained from the difference between the values of the coefficients measured at angles of sideslip of ±5°. These data indicate that with tower on, the model was statically directionally stable for angles of attack from about -18° to 18°. It is also shown that the disk generally increased the directional stability over the angle-of-attack range.

The data of figure 8 show that the command module, in the exit attitude, was trimmed in pitch at an angle of attack of about 54° and was statically stable longitudinally about this trim point over an angle-of-attack range from about 0° to 100°. The command module in the reentry attitude (see fig. 9) was trimmed in pitch at an angle of attack of about 28° and was statically stable longitudinally about this trim point over an angle-of-attack range from about 0° to 80°. The lateral data of figure 11 show that in the exit attitude the command module had neutral static directional stability up to an angle of attack of about 40° and then became stable up to an angle of attack of about 110°. The command module in the reentry attitude had positive C_{n_β} up to an angle of attack of about 78° before becoming unstable (see fig. 12).

Dynamic Derivatives

The variation of the in-phase and out-of-phase derivatives with angle of attack for the various model configurations tested are presented in figures 13 to 17. Also presented with the in-phase data for the purpose of comparison are static force-test data (k = 0). These data show generally good agreement between the static and dynamic force-test results.

The data of figure 13(b) show that the launch-escape vehicle without the disk had stable values of damping in pitch $-\left(C_{m_q} + C_{m_{\dot{\alpha}}}\right)$ over the angle-of-attack range tested (-30° to 60°) but that the damping was low near zero angle of attack. The data also show that the model with the disk had unstable values of damping in pitch for angles of attack from about -5° to 5°. The yawing oscillation data presented in figure 14(b) show that the launch-escape vehicle had unstable values of damping in yaw $\left(C_{n_r} - C_{n_{\dot{\beta}}} \cos \alpha\right)$ for angles of attack from about -10° to 10° with or without the disk.

In general, the command module in the exit attitude had very little damping in pitch (see fig. 15(b)) or yaw (see fig. 16(b)).

The data of figure 17 indicate that large increases in the amplitude of the oscillation tend to increase the damping in pitch near zero angle of attack for the launch-escape vehicle.

CONCLUDING REMARKS

A force-test investigation has been conducted at the Langley Research Center to provide information on the longitudinal and lateral stability characteristics at low subsonic speeds of a 1/7-scale model of the Apollo launch-escape vehicle and command module. The results of the investigation show that the model in all configurations had at least neutral static longitudinal and directional stability near zero angle of attack. The launch-escape vehicle had stable values of damping in pitch but unstable values of damping in yaw near zero angle of attack while the command module in the exit attitude had very small values of damping in pitch and yaw. Increasing the amplitude of the oscillation tended to increase the damping in pitch near zero angle of attack for the launch-escape vehicle.

Langley Research Center,
National Aeronautics and Space Administration,
Langley Station, Hampton, Va., July 10, 1963.

REFERENCES

1. Morgan, James R., and Fournier, Roger H.: Static Longitudinal Aerodynamic Characteristics of a 0.07-Scale Model of a Proposed Apollo Spacecraft at Mach Numbers of 1.57 to 4.65. NASA TM X-603, 1961.

2. Pearson, Albin O.: Wind-Tunnel Investigation of the Static Longitudinal Aerodynamic Characteristics of Models of Reentry and Atmospheric-Abort Configurations of a Proposed Apollo Spacecraft at Mach Numbers From 0.30 to 1.20. NASA TM X-604, 1961.

3. Hewes, Donald E.: Low-Subsonic Measurements of the Static and Oscillatory Lateral Stability Derivatives of a Sweptback-Wing Airplane Configuration at Angles of Attack From -10° to 90°. NASA MEMO 5-20-59L, 1959.

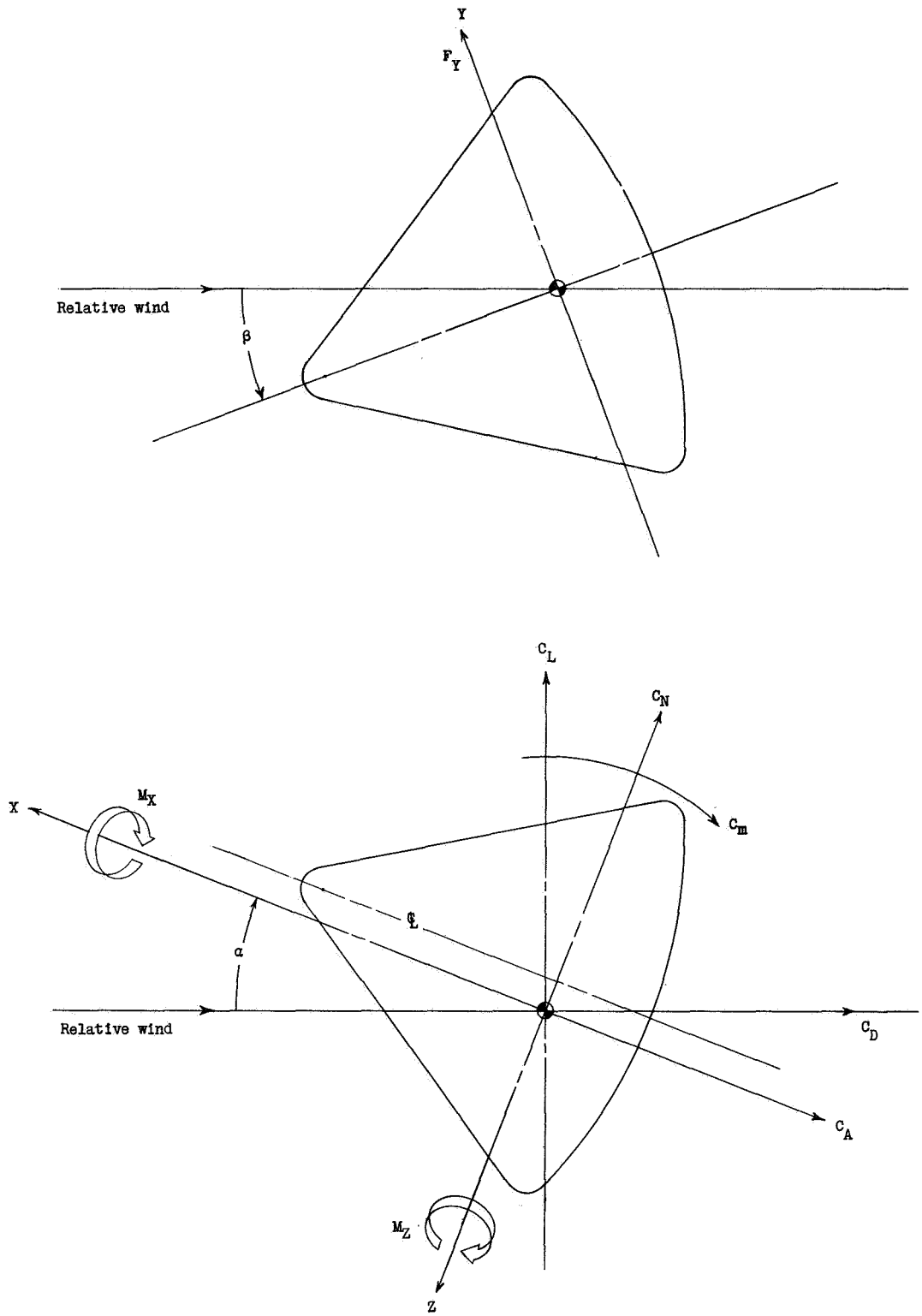

Figure 1.- System of axes used in investigation. Arrows indicate positive directions.

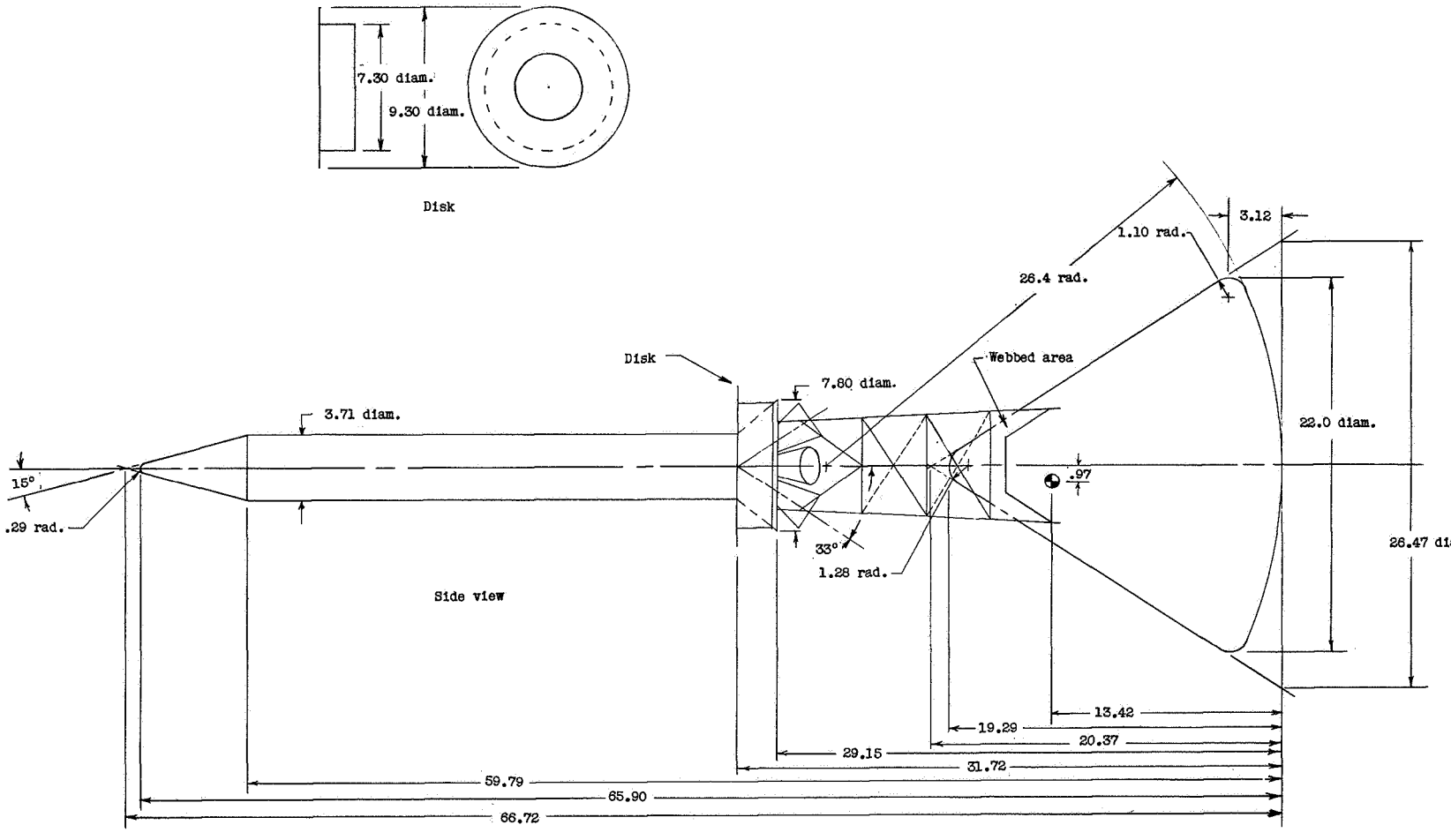

(a) Launch-escape vehicle.

Figure 2.- Sketches of model used in investigation. All dimensions are in inches unless otherwise specified.

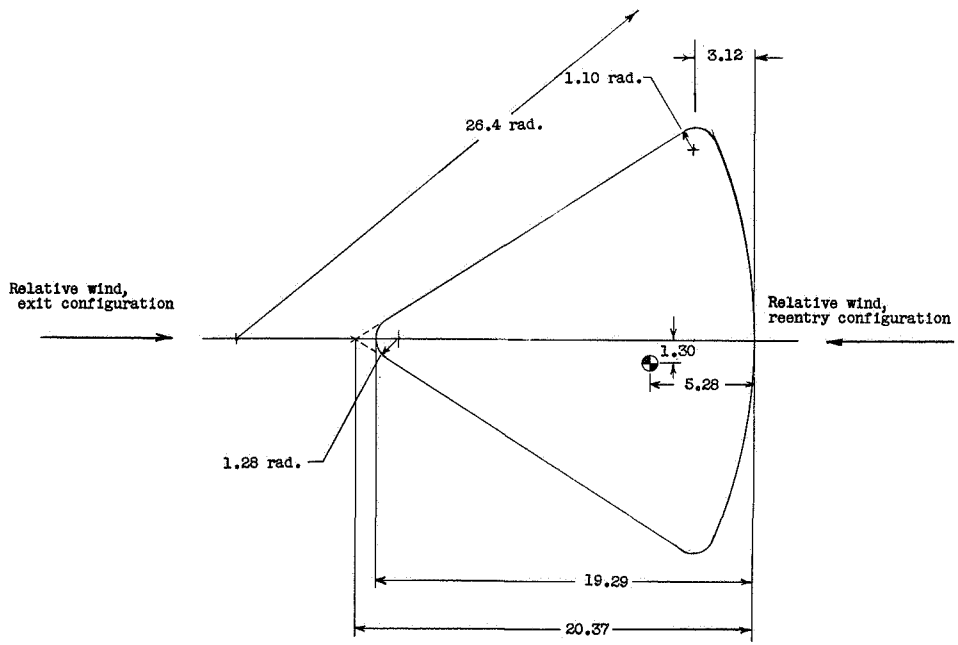

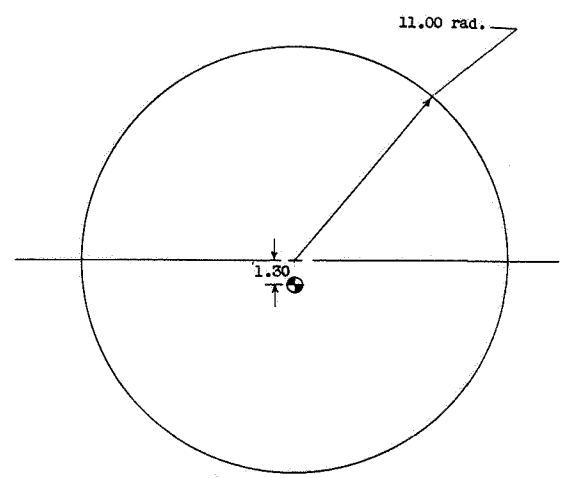

(b) Command-module configuration.

Figure 2.- Concluded.

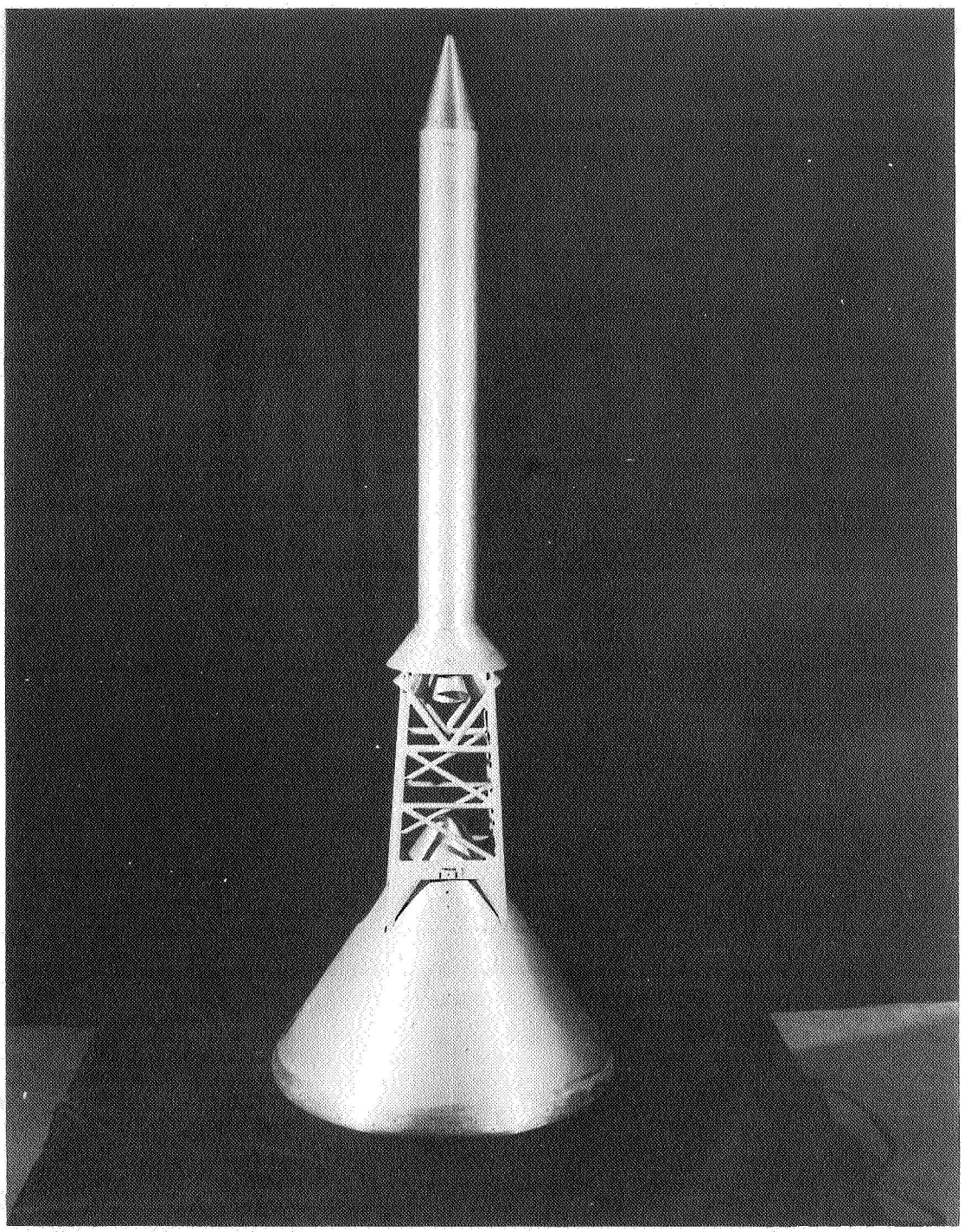

(a) Launch-escape vehicle. L-62-7940

Figure 3.- Photographs of model configurations tested.

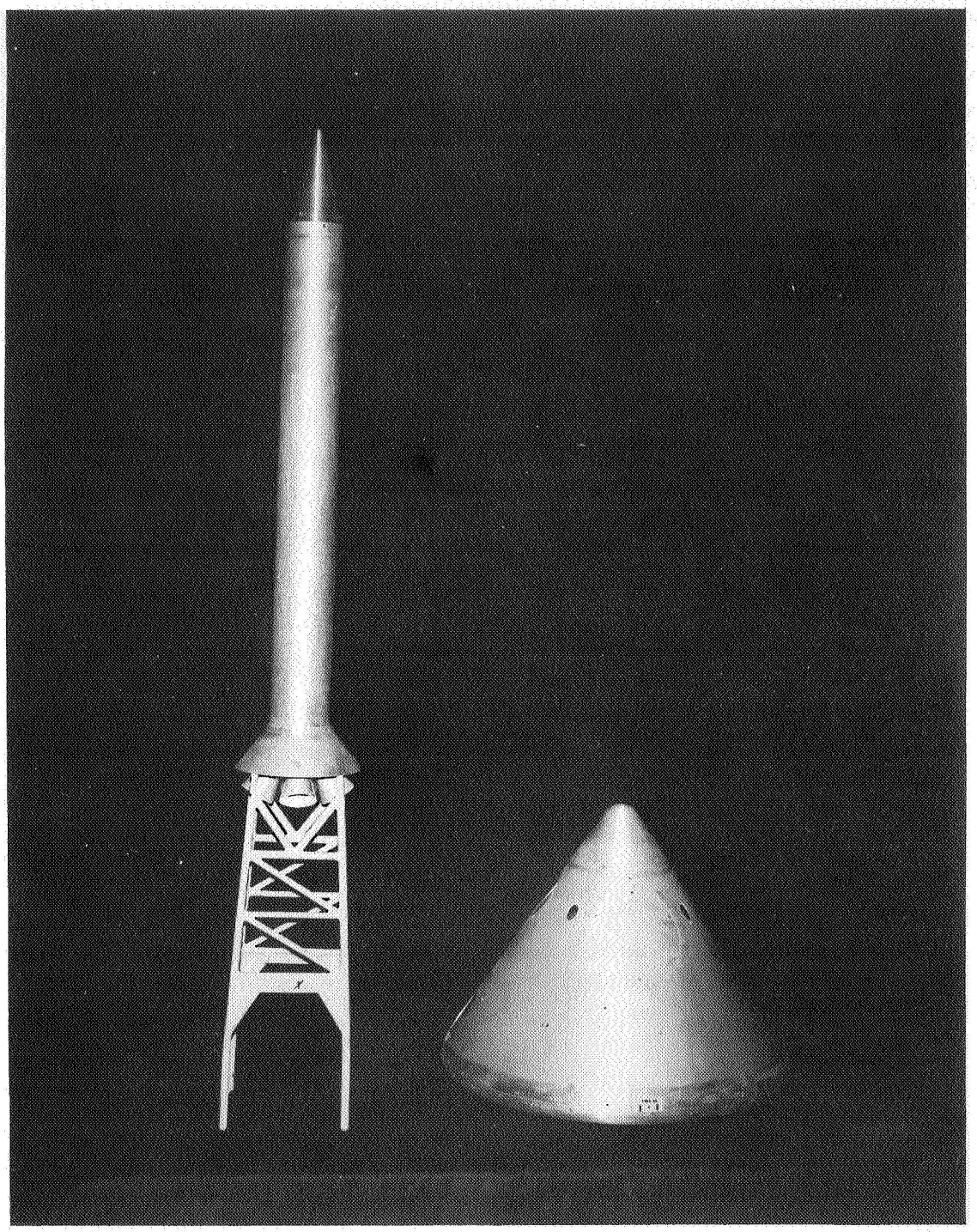

(b) Escape tower removed from command module. L-62-7936

Figure 3.- Continued.

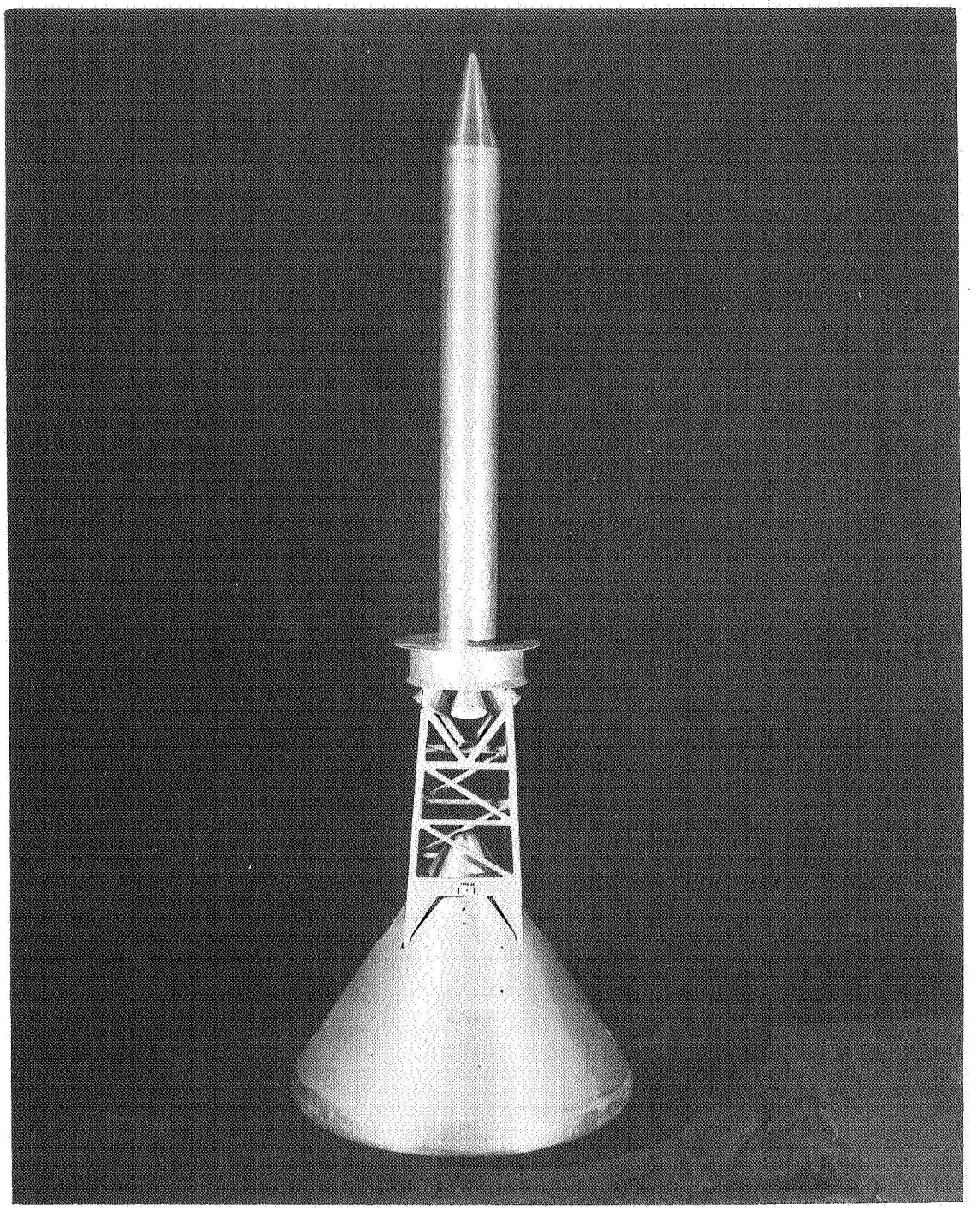

(c) Launch-escape vehicle with disk. L-62-7931

Figure 3.- Concluded.

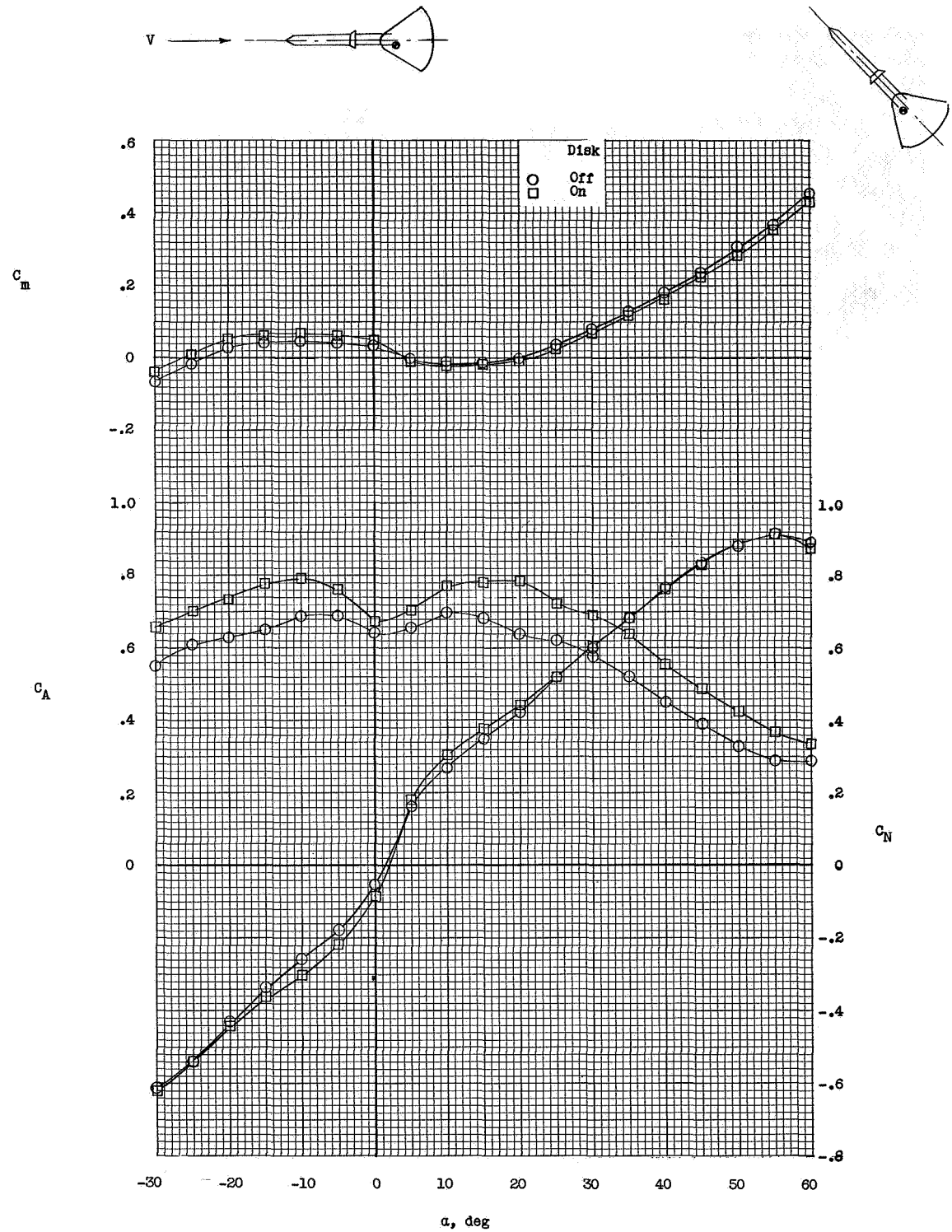

Figure 4.- Static longitudinal stability characteristics of launch-escape vehicle.

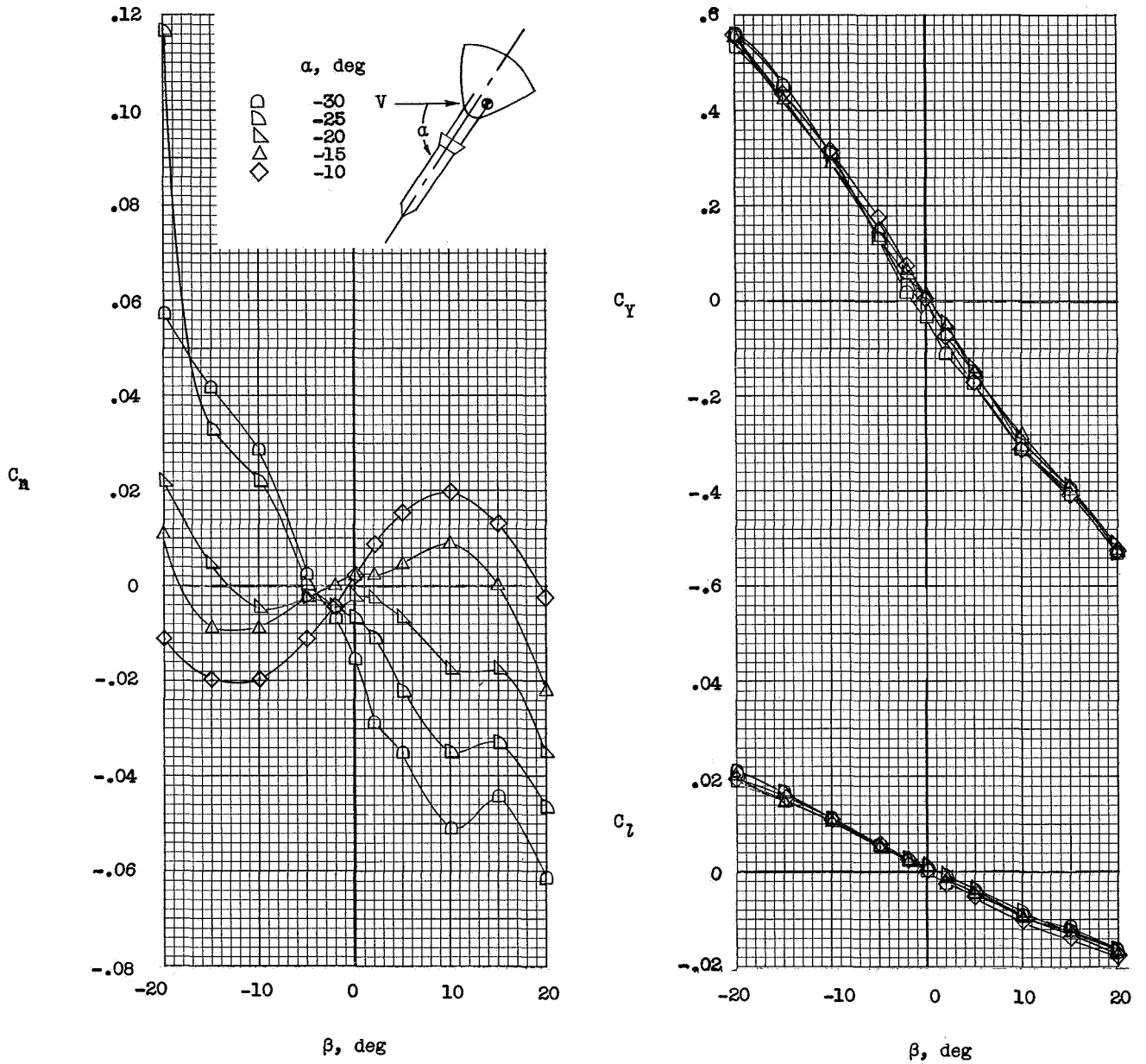

Figure 5.- Variation of static lateral stability characteristics with angle of sideslip for launch-escape vehicle without disk.

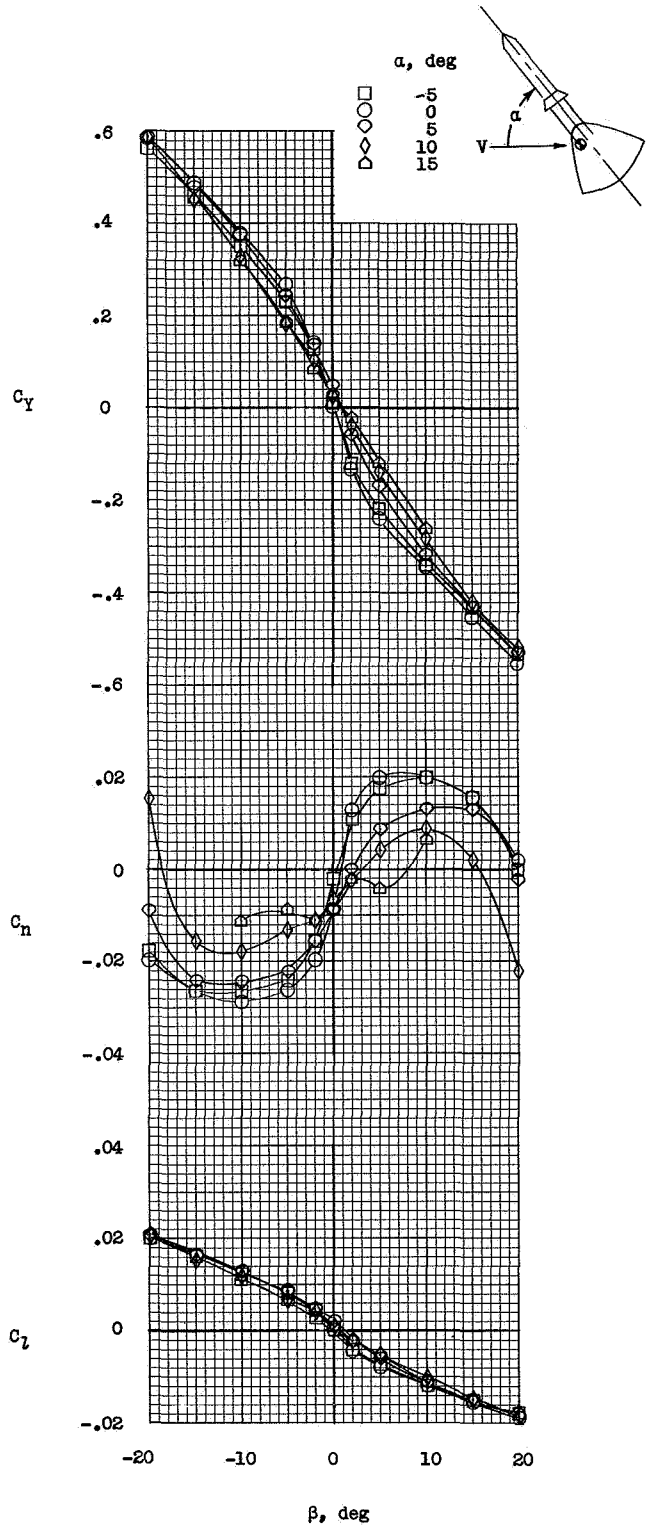

Figure 5.- Continued.

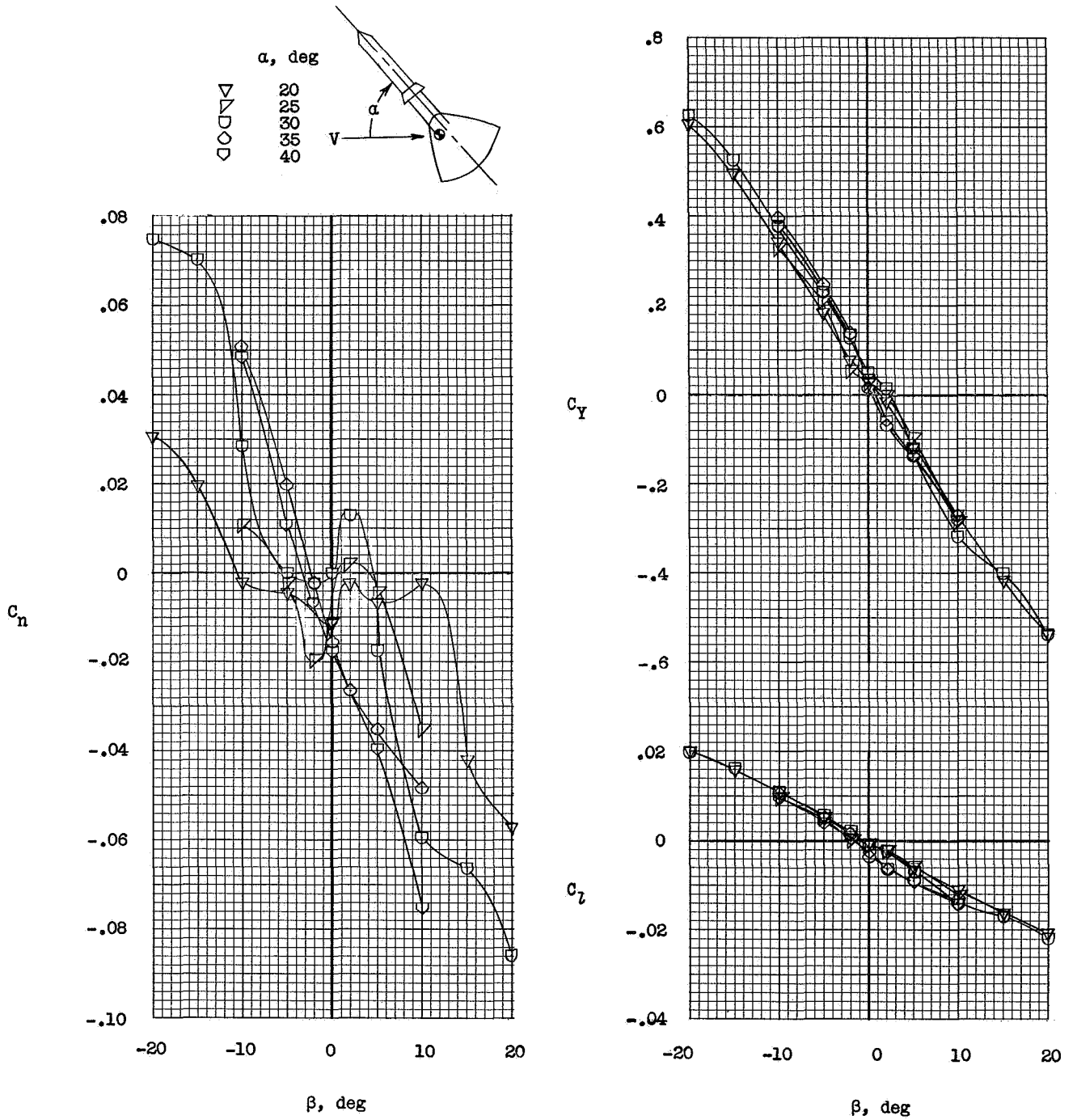

Figure 5.- Continued.

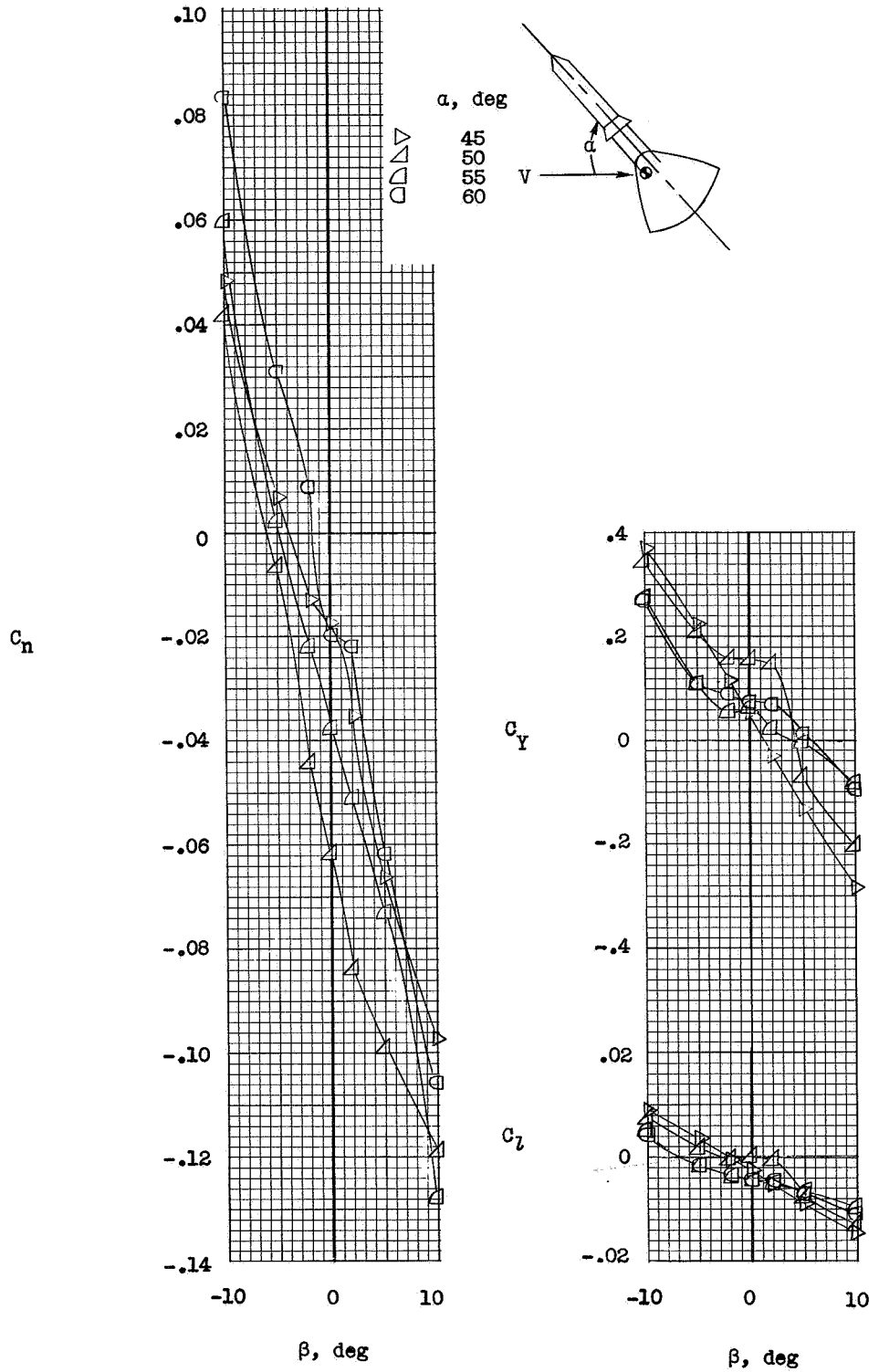

Figure 5.- Concluded.

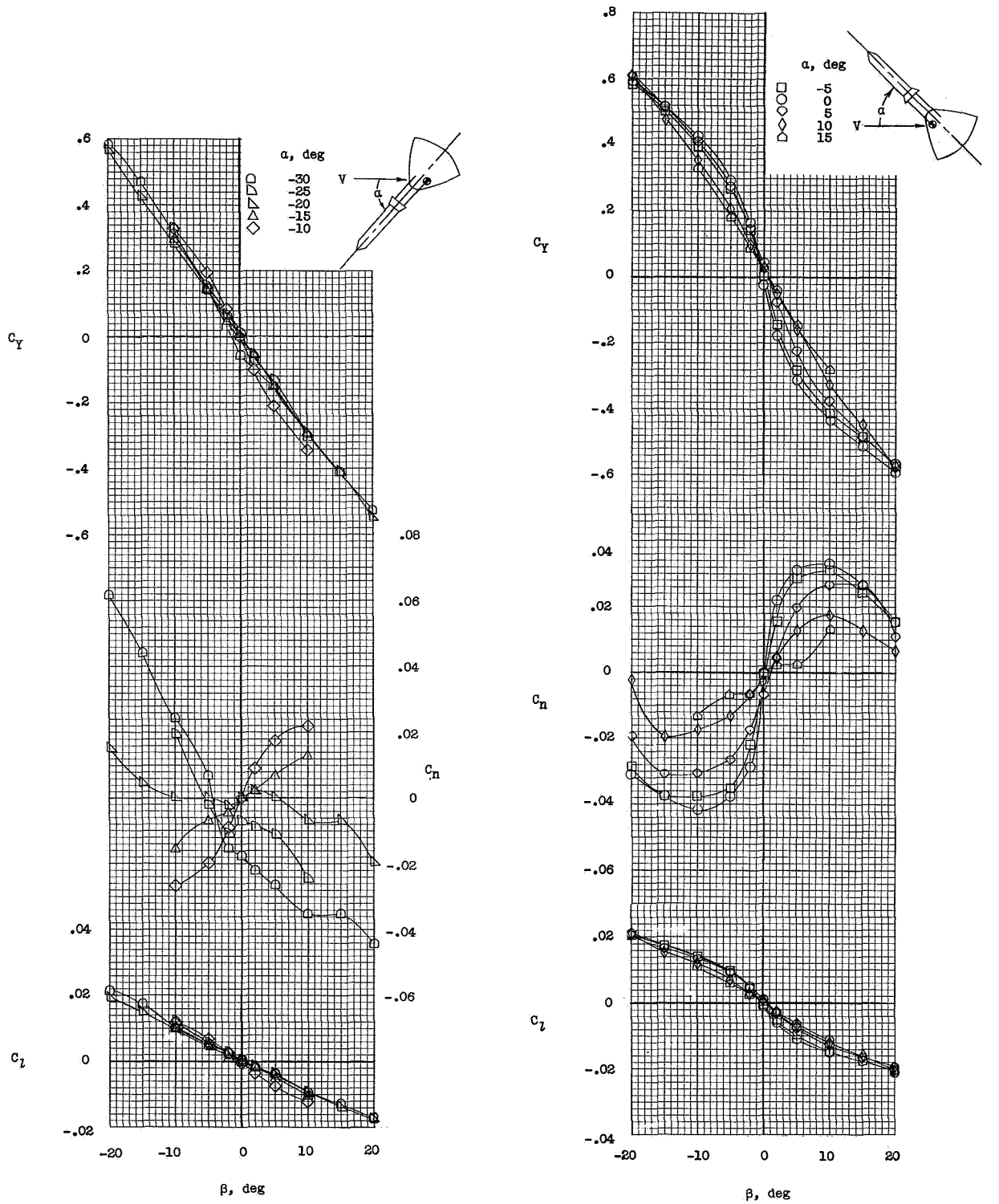

Figure 6.- Variation of static lateral stability characteristics with angle of sideslip for launch-escape vehicle with disk.

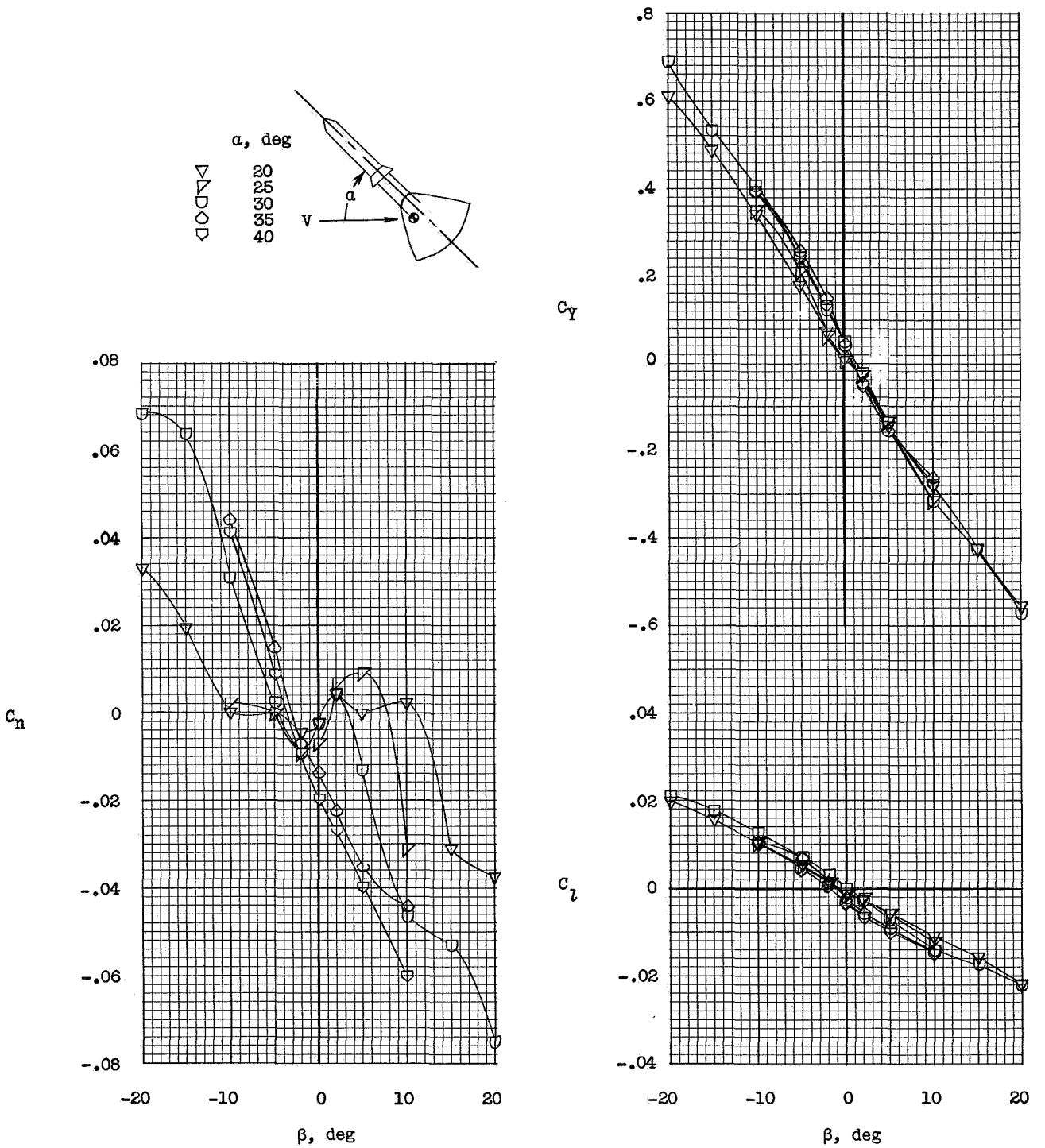

Figure 6.- Continued.

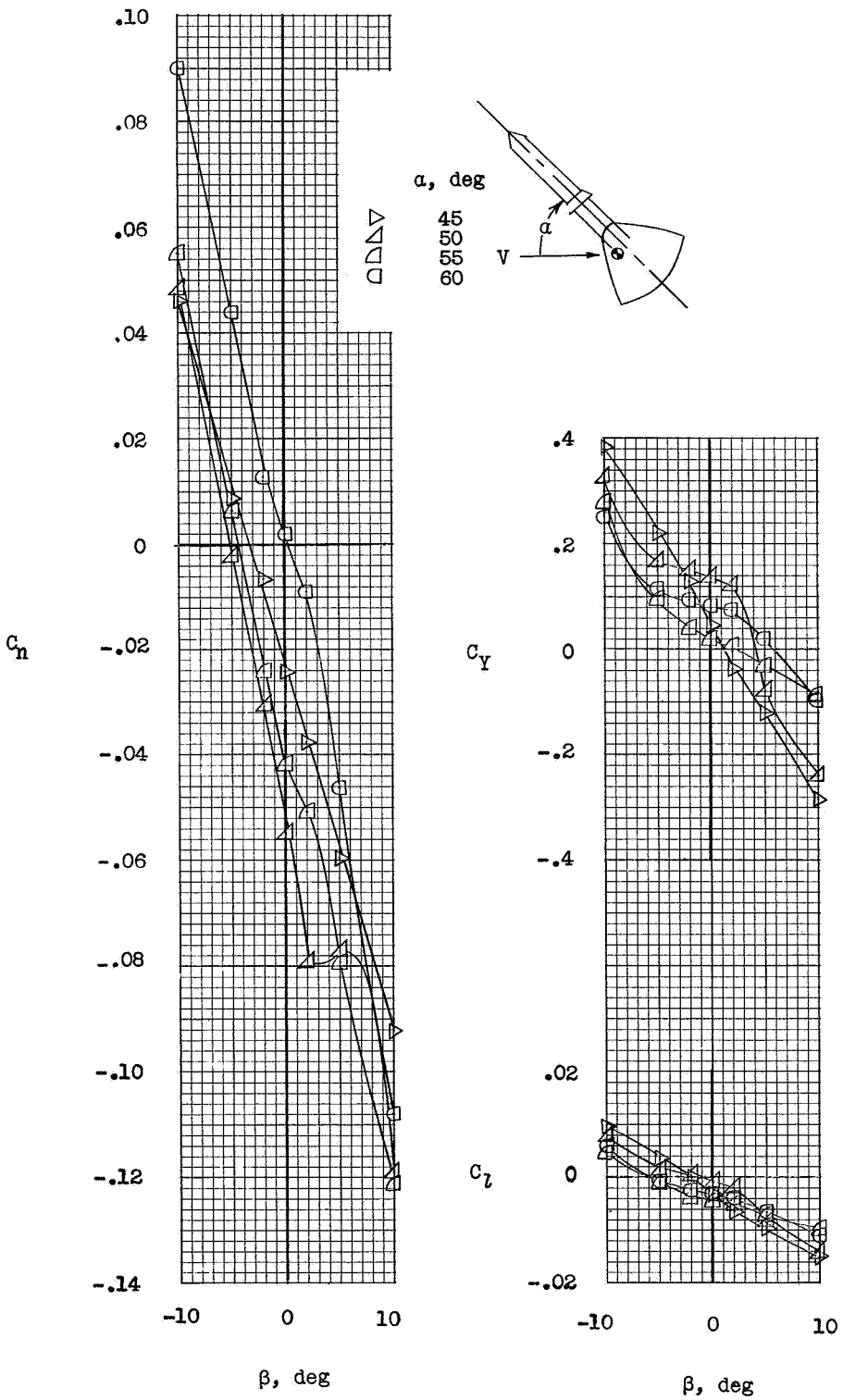

Figure 6.- Concluded.

Figure 7.- Variation of static sideslip derivatives with angle of attack for launch-escape vehicle.

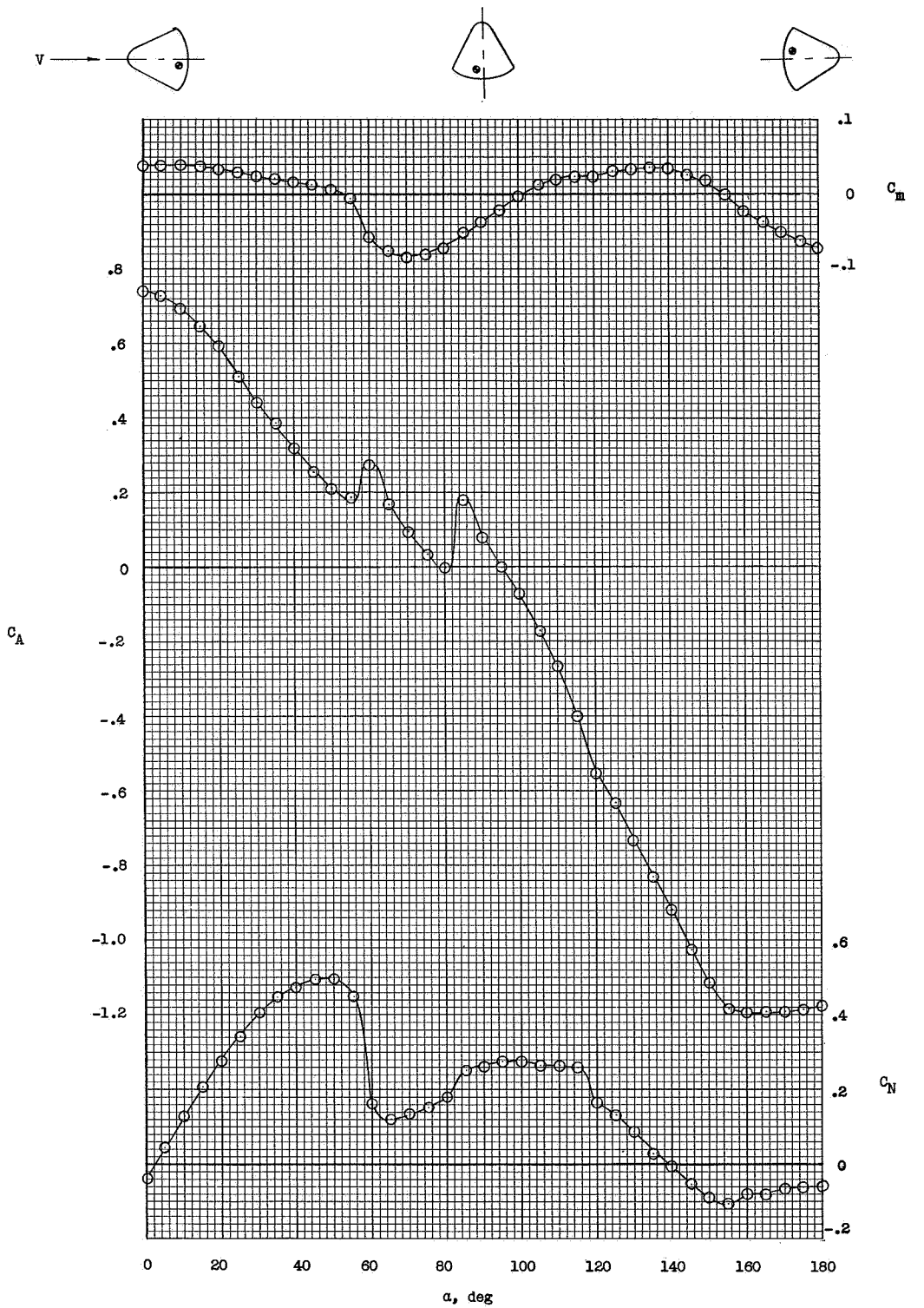

Figure 8.- Static longitudinal stability characteristics of command module in exit attitude.

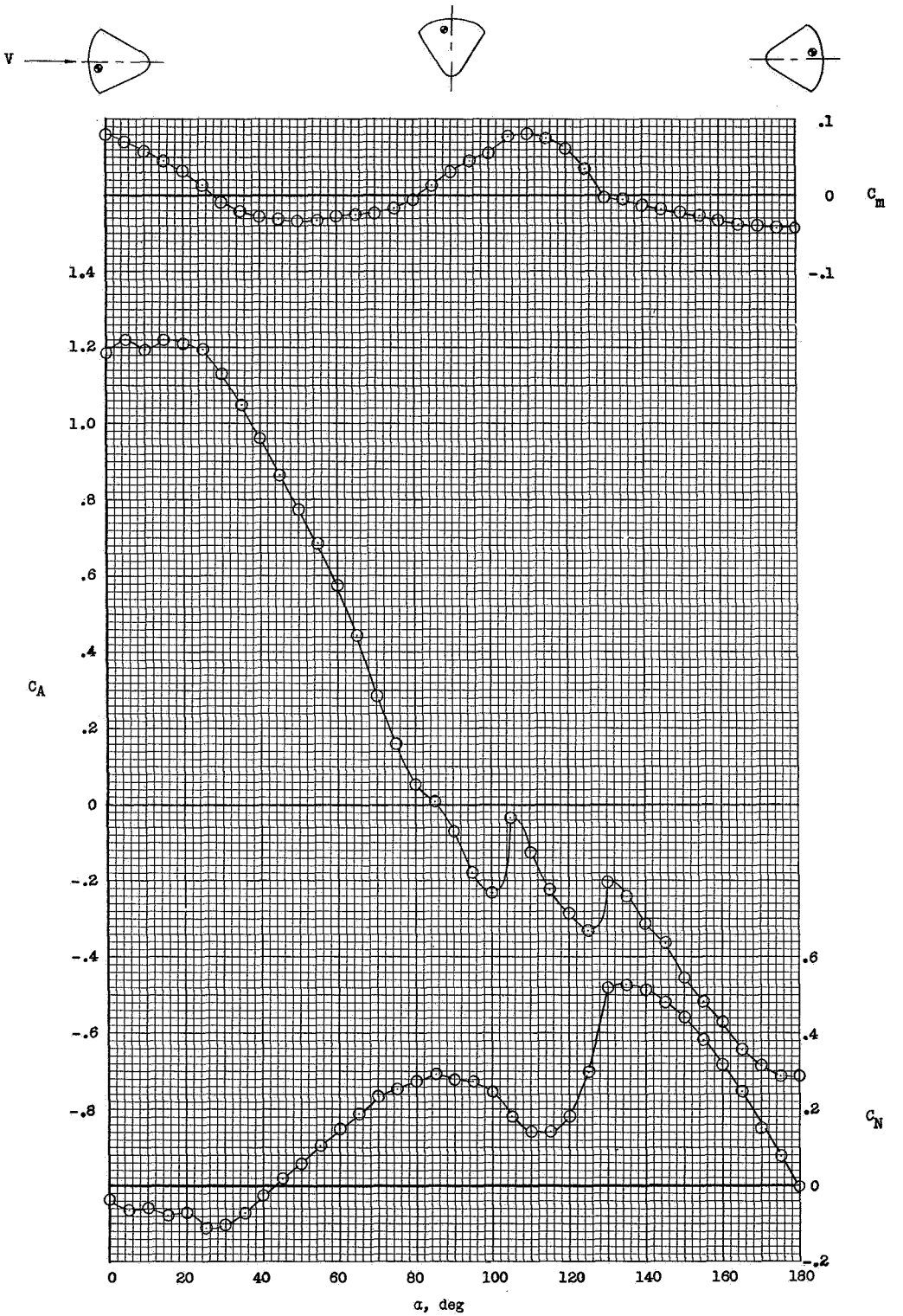

Figure 9.- Static longitudinal stability characteristics of command module in reentry attitude.

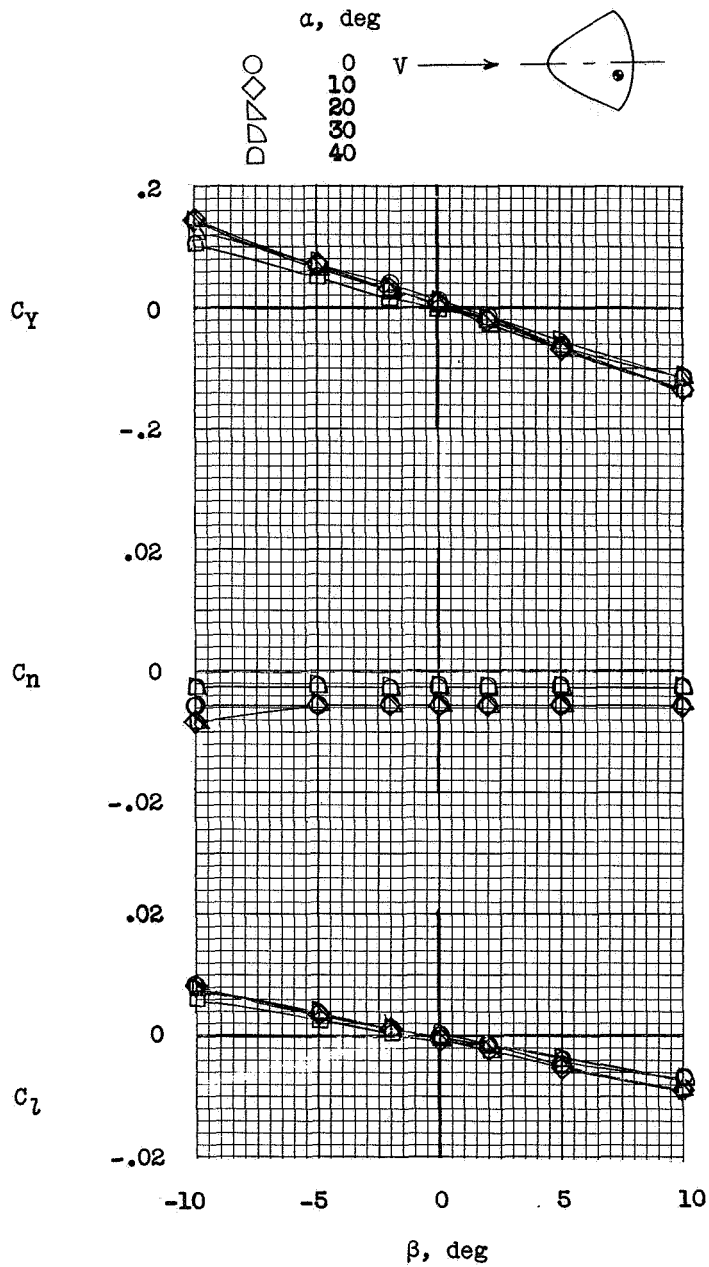

Figure 10.- Variation of static lateral stability characteristics with angle of sideslip for command module in exit attitude.

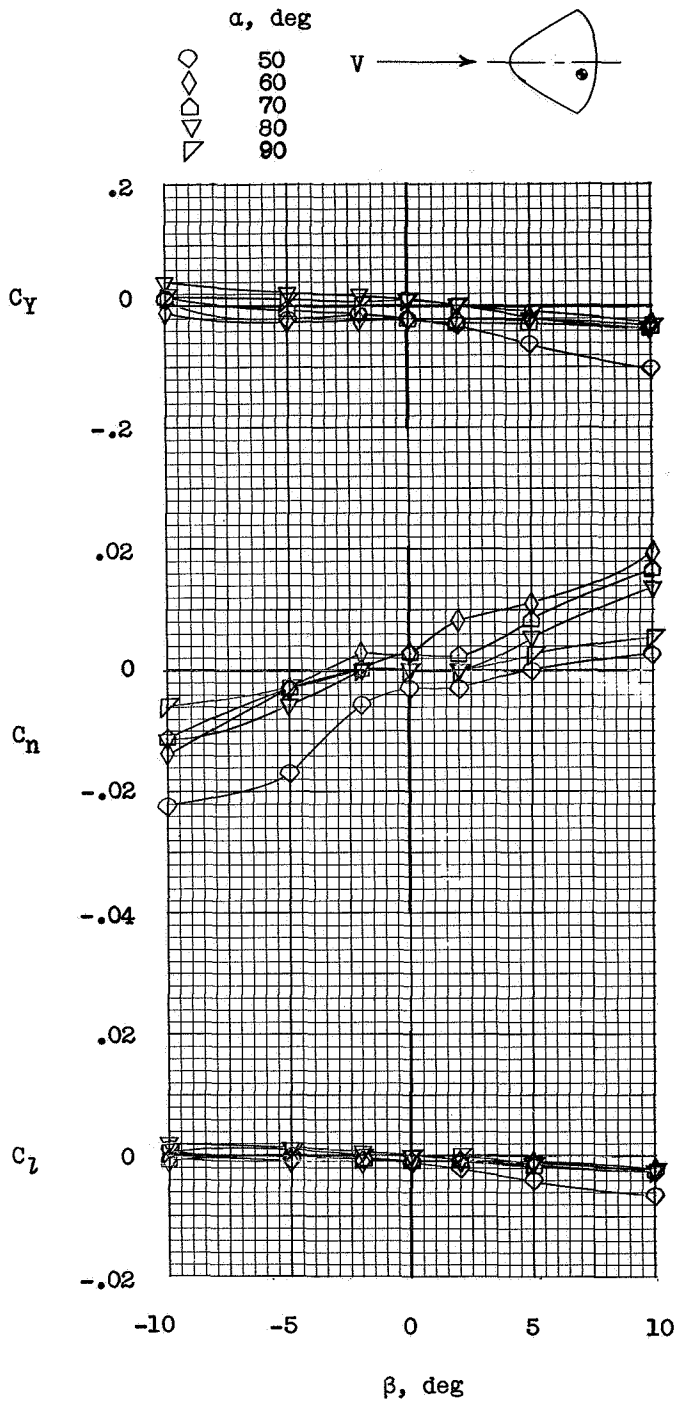

Figure 10.- Continued.

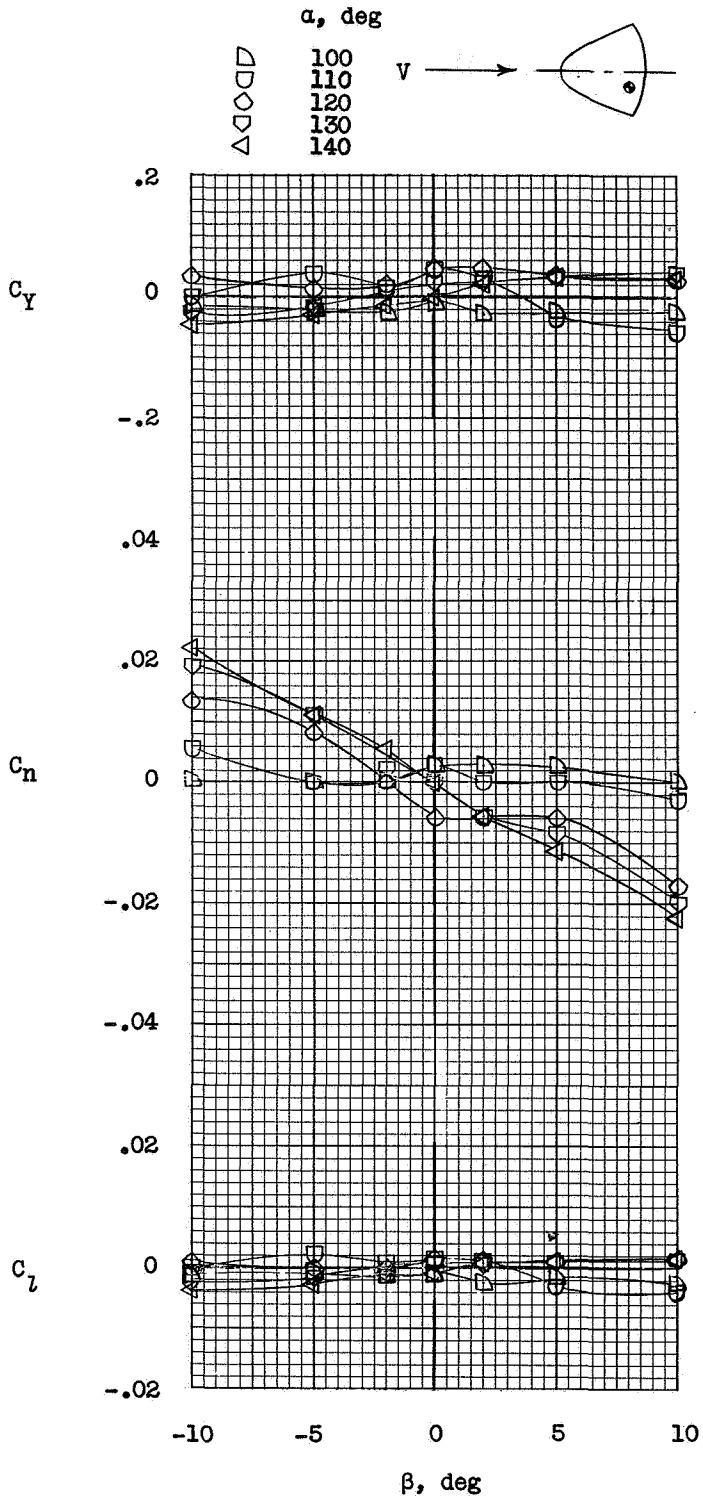

Figure 10.- Continued.

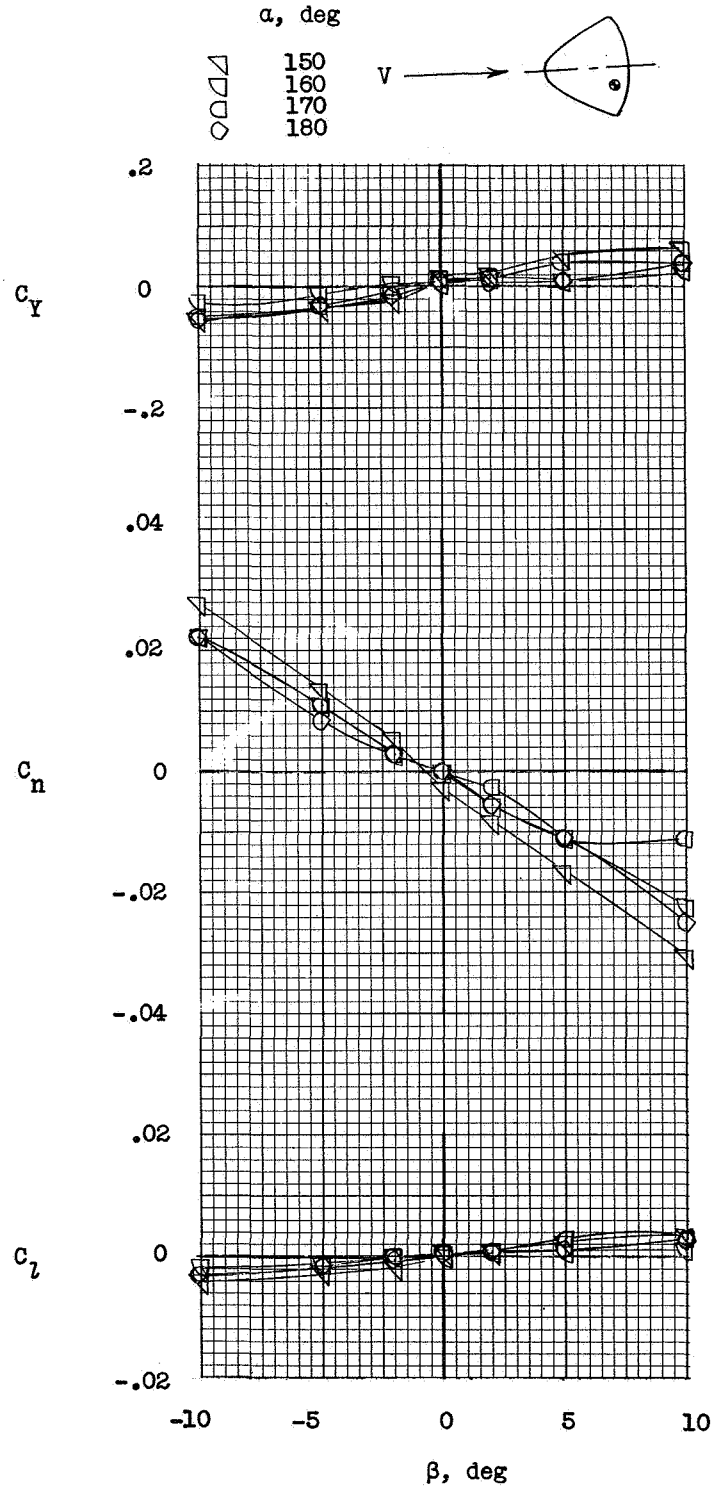

Figure 10.- Concluded.

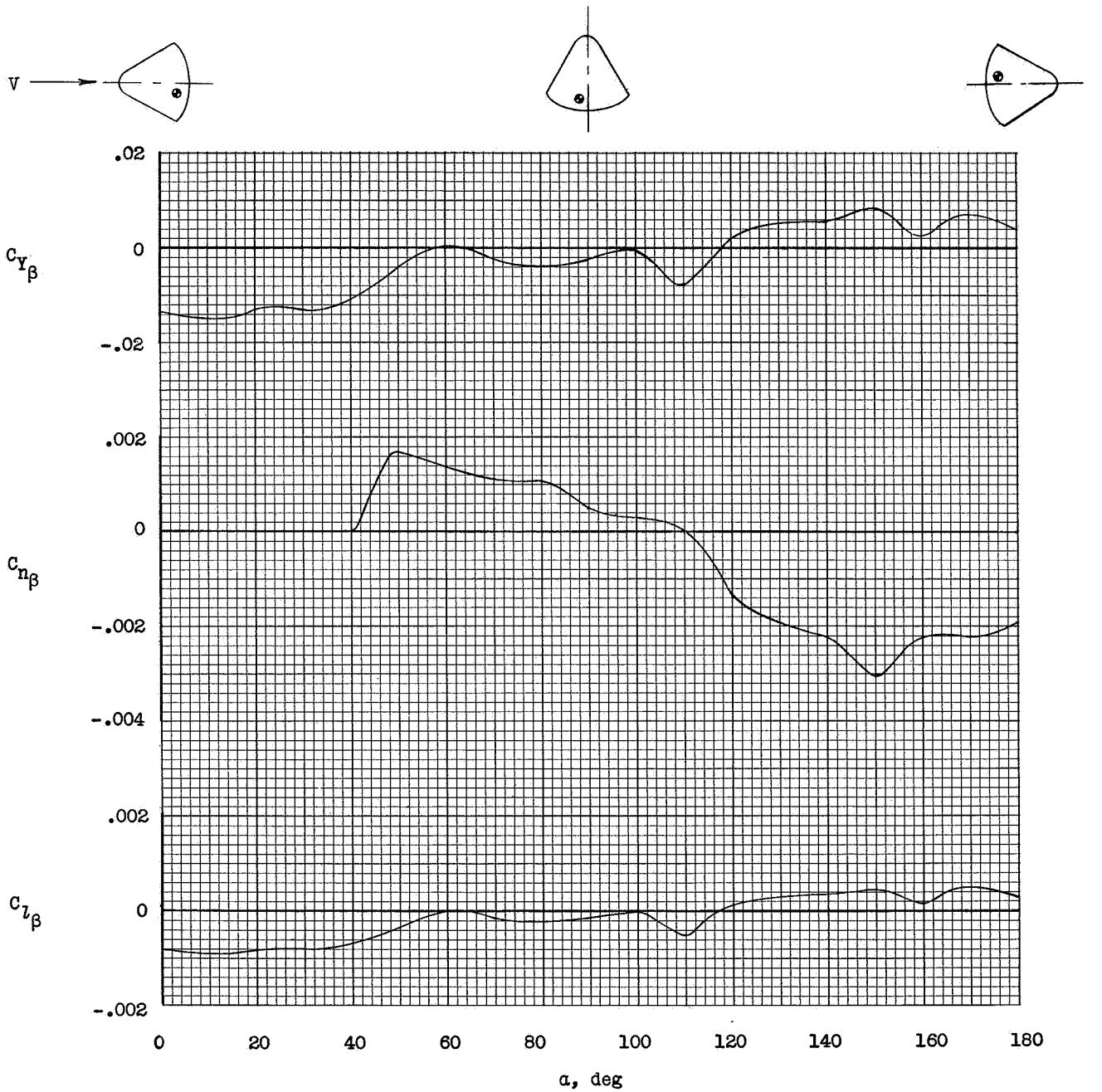

Figure 11.- Variation of static sideslip derivatives with angle of attack for command module in exit attitude.

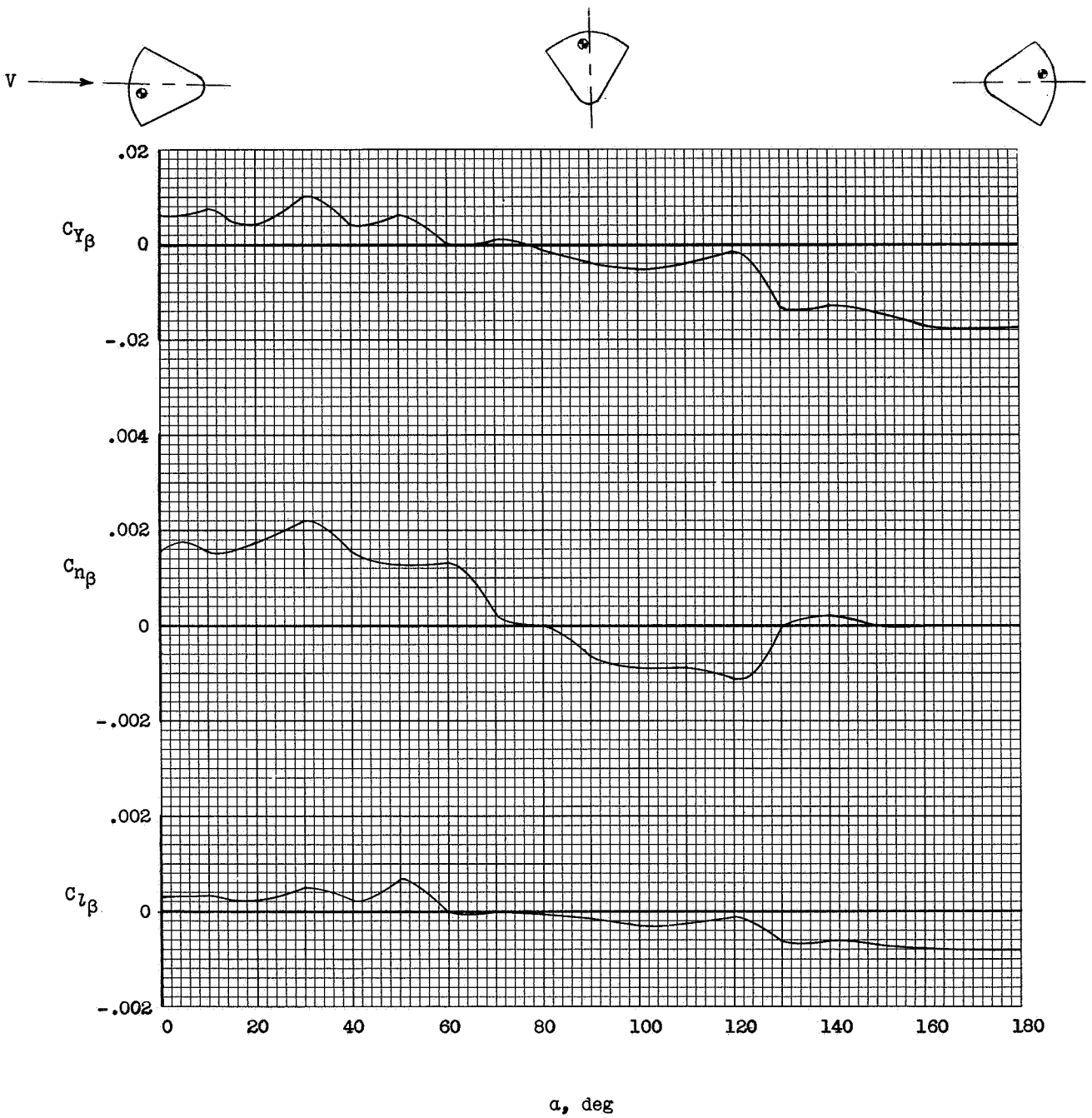

Figure 12.- Variation of static sideslip derivatives with angle of attack for command module in reentry attitude.

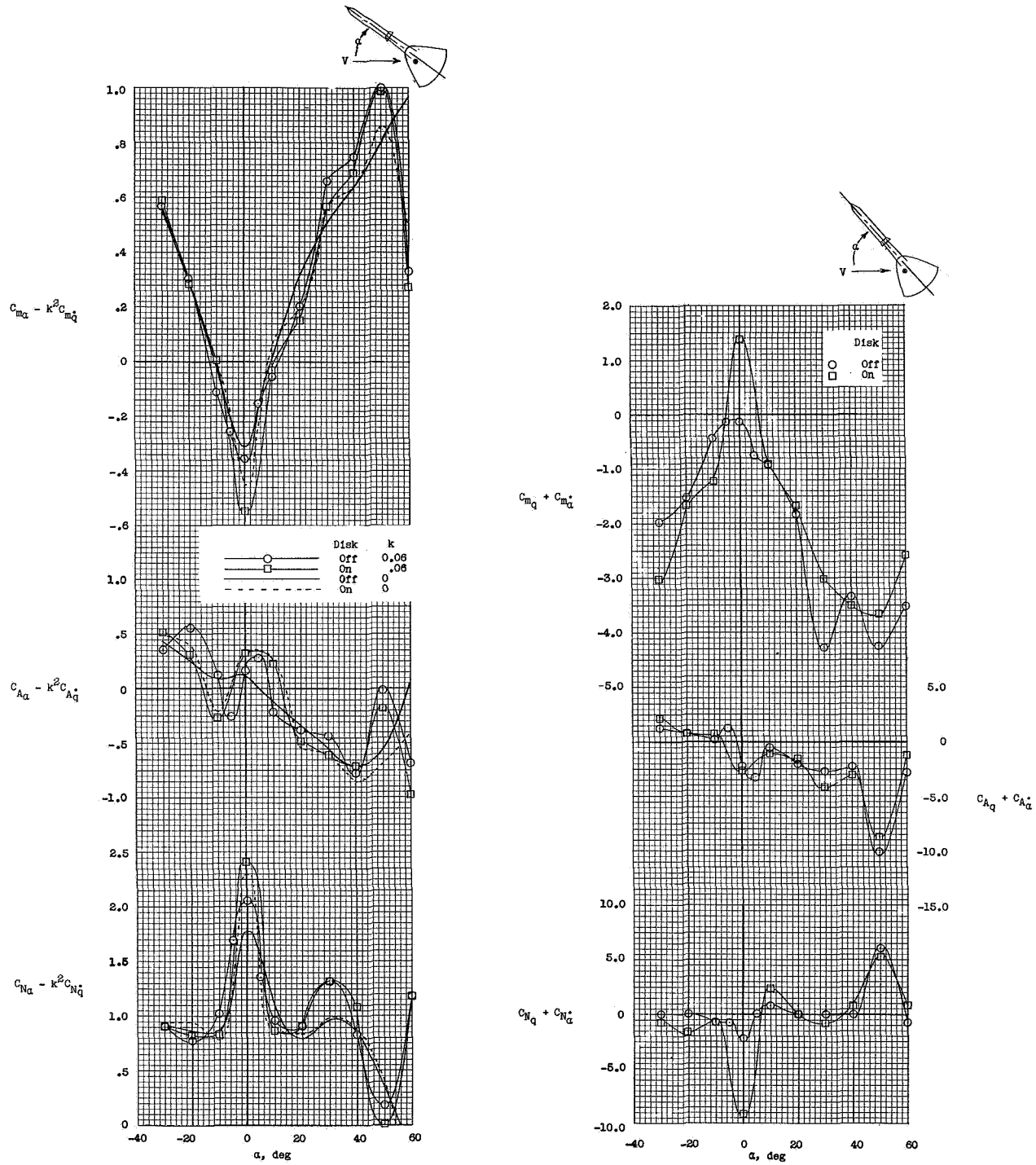

(a) In-phase derivatives with displacement. (b) Out-of-phase derivatives with displacement.

Figure 13.- Longitudinal oscillatory stability derivatives for launch-escape vehicle.

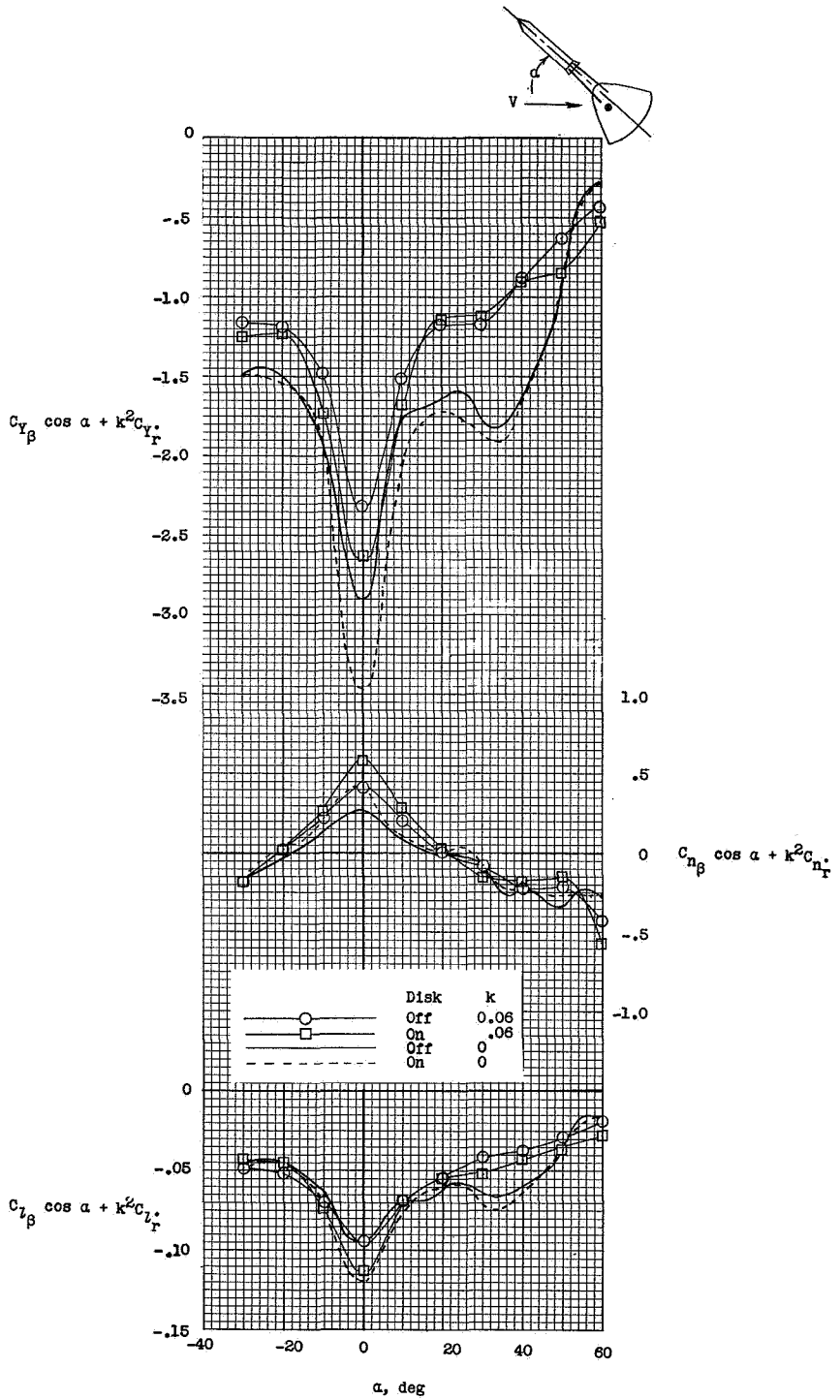

(a) In-phase derivatives with displacement.

Figure 14.- Yawing oscillatory derivatives for launch-escape vehicle.

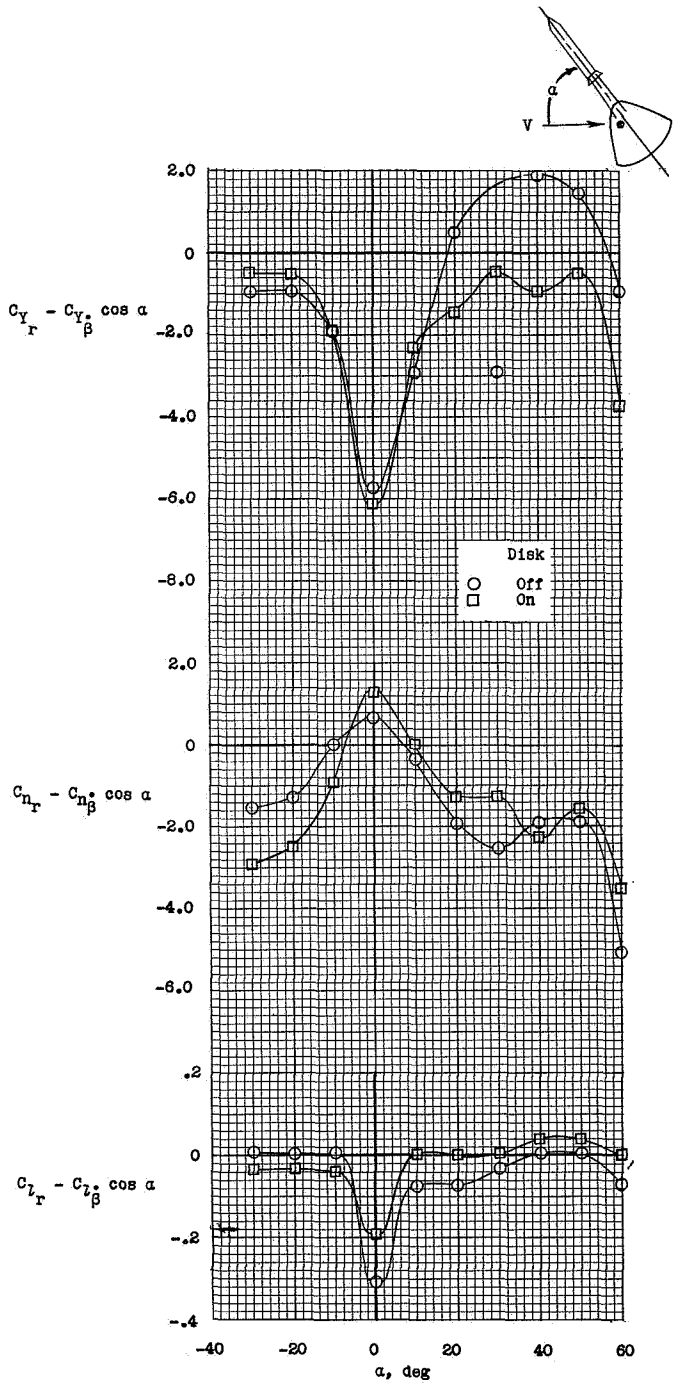

(b) Out-of-phase derivatives with displacement.

Figure 14.- Concluded.

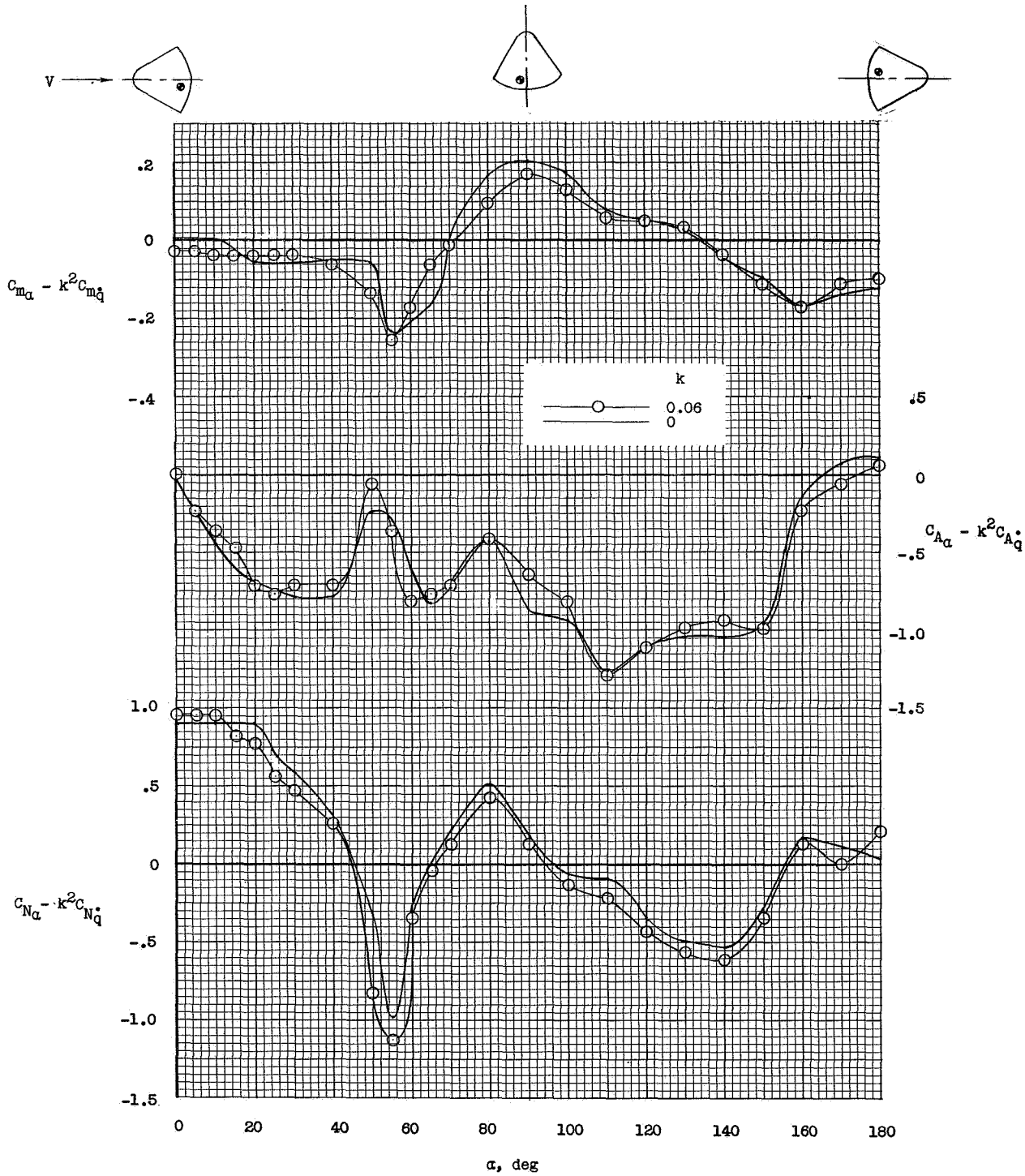

(a) In-phase derivatives with displacement.

Figure 15.- Longitudinal oscillatory derivatives for command module in exit attitude.

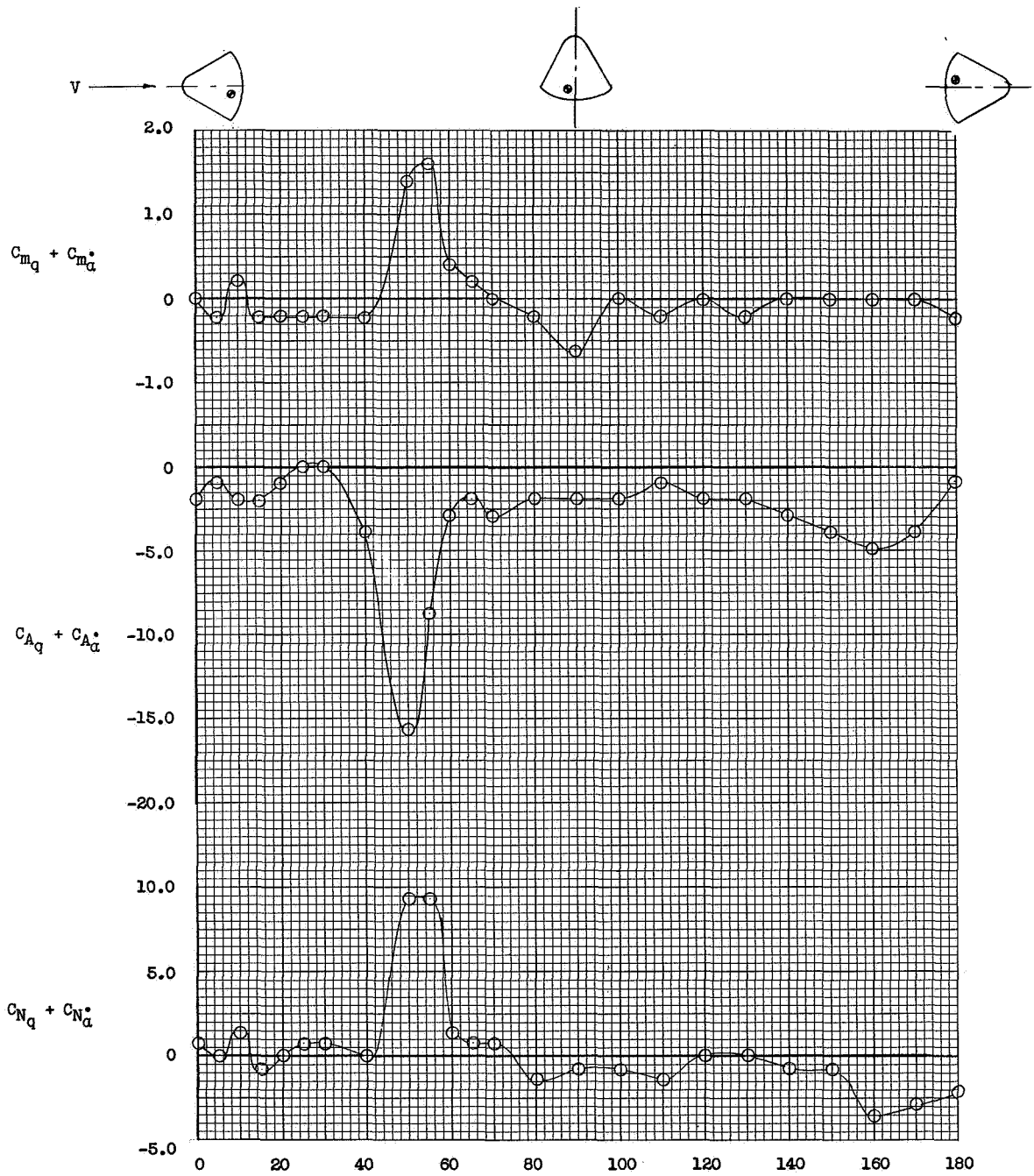

(b) Out-of-phase derivatives with displacement.

Figure 15.- Concluded.

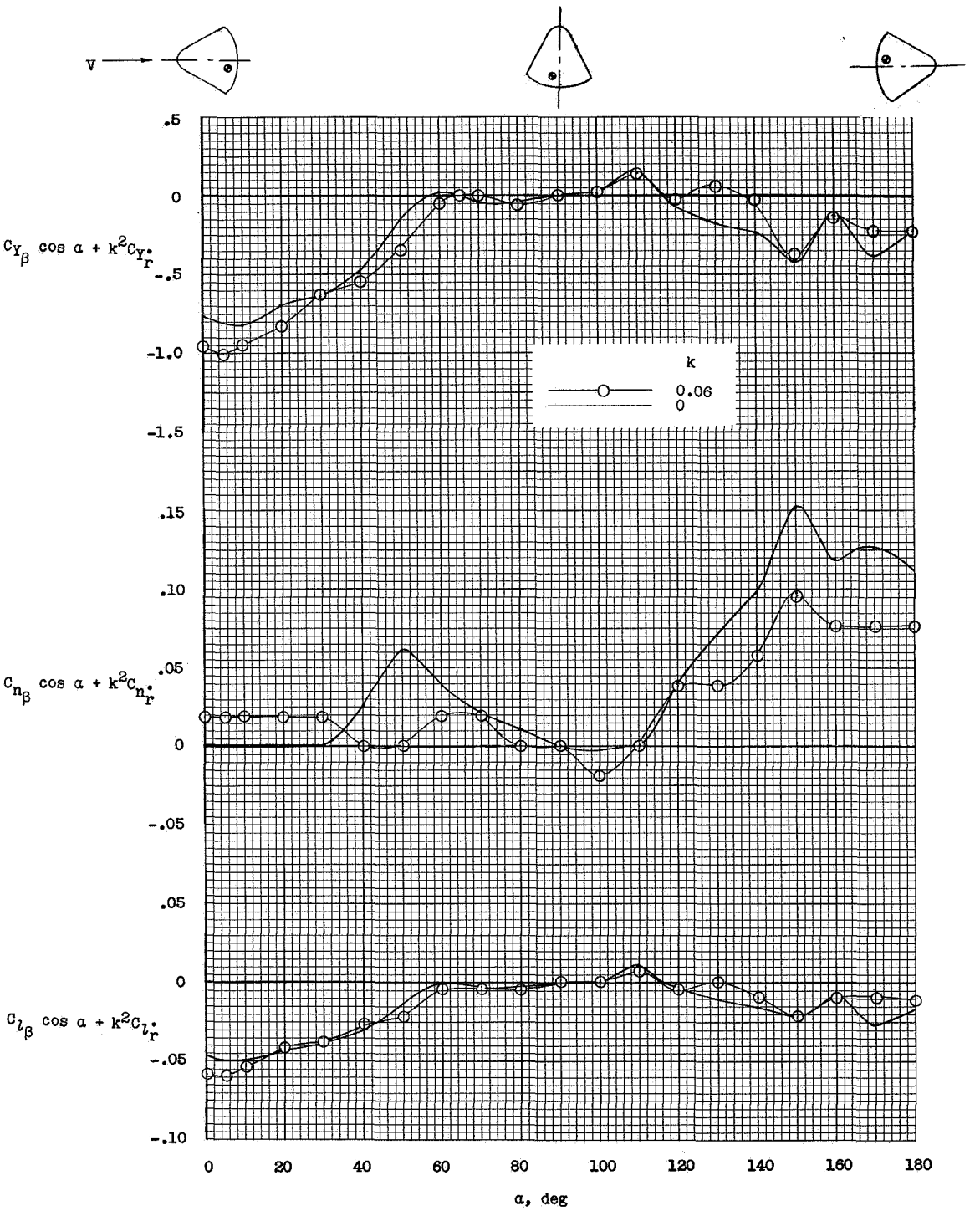

(a) In-phase derivatives with displacement.

Figure 16.- Yawing oscillatory derivatives for command module in exit attitude.

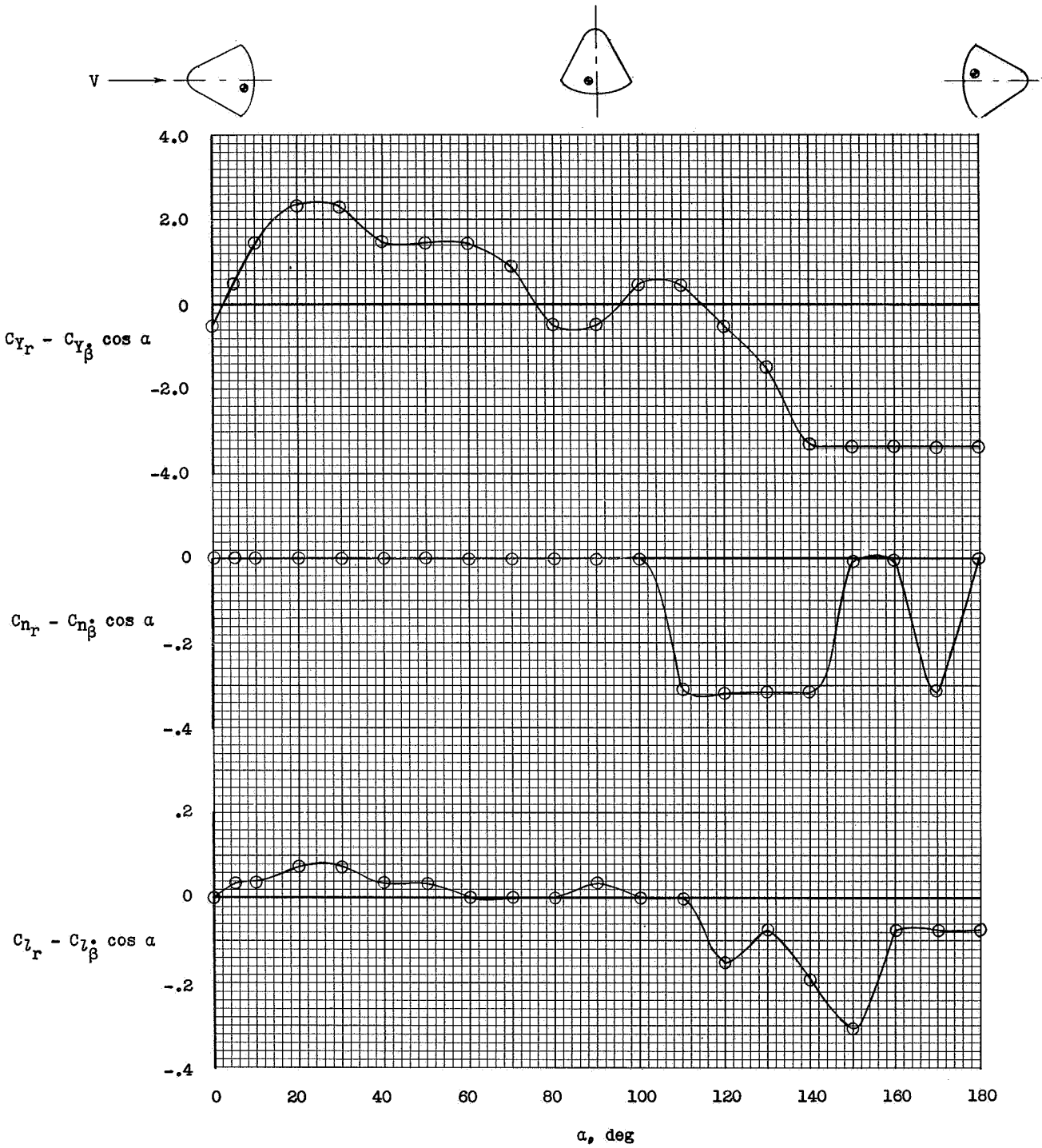

(b) Out-of-phase derivatives with displacement.

Figure 16.- Concluded.

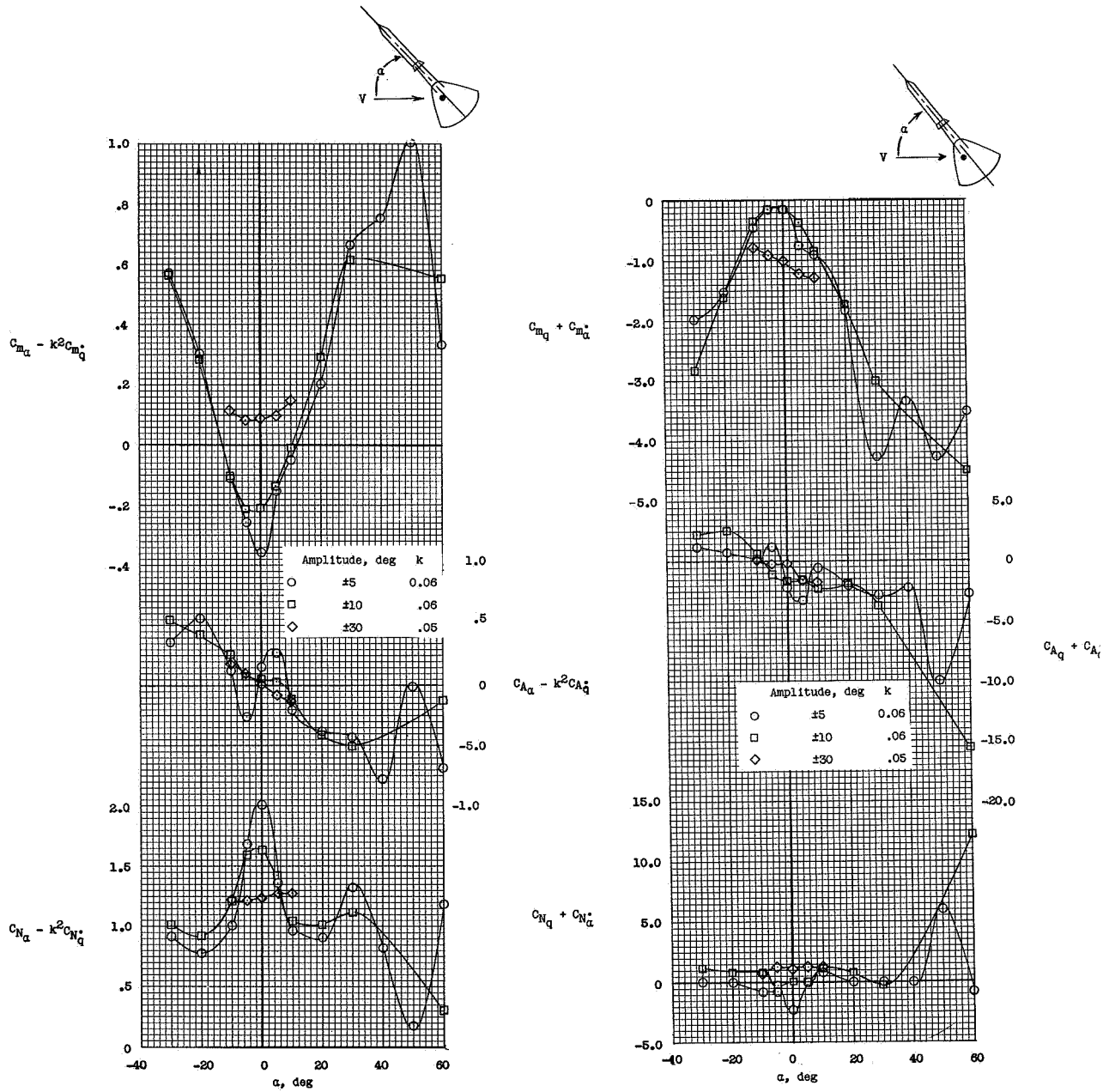

(a) In-phase derivatives with displacement. (b) Out-of-phase derivatives with displacement.

Figure 17.- Effect of amplitude on longitudinal oscillatory stability derivatives for command module with escape tower and without disk.